

Durham Research Online

Deposited in DRO:

07 June 2017

Version of attached file:

Accepted Version

Peer-review status of attached file:

Peer-reviewed

Citation for published item:

Li, Y. and Selby, D. and Condon, D. and Tapster, S. (2017) 'Cyclic magmatic-hydrothermal evolution in porphyry systems : high-precision U-Pb and Re-Os geochronology constraints from the Tibetan Qulong porphyry Cu-Mo deposit.', *Economic geology*, 112 (6). pp. 1419-1440.

Further information on publisher's website:

<https://doi.org/10.5382/econgeo.2017.4515>

Publisher's copyright statement:

Additional information:

Use policy

The full-text may be used and/or reproduced, and given to third parties in any format or medium, without prior permission or charge, for personal research or study, educational, or not-for-profit purposes provided that:

- a full bibliographic reference is made to the original source
- a [link](#) is made to the metadata record in DRO
- the full-text is not changed in any way

The full-text must not be sold in any format or medium without the formal permission of the copyright holders.

Please consult the [full DRO policy](#) for further details.

Cyclic magmatic-hydrothermal evolution in porphyry systems: High-precision U-Pb and Re-Os geochronology constraints from the Tibetan Qulong porphyry Cu-Mo deposit

Yang Li ^{1*}, David Selby ¹, Daniel Condon ² and Simon Tapster ²

¹Department of Earth Sciences, Durham University, DH1 3LE, Durham, UK

²NERC Isotope Geosciences Laboratory, British Geological Survey, NG12 5GG, Nottingham, UK

*Corresponding author Email, li.yang@durham.ac.uk; cugliyang@126.com, Current address, Department of Geology and Geophysics, Yale University, New Haven, Connecticut, 06511, USA

Keywords, High precision geochronology; U-Pb; Re-Os; Cyclic; Porphyry Copper System; Qulong.

Abstract

We present high-precision chemical abrasion isotope dilution thermal ionization mass spectrometry (CA-ID-TIMS) U-Pb zircon and isotope dilution negative thermal ionization mass spectrometry (ID-N-TIMS) Re-Os molybdenite geochronology of the world-class Tibetan Qulong porphyry Cu-Mo deposit. The data is used to constrain the timing, duration and yield implications of the ore-forming processes. The U-Pb data suggest that the pre-ore Rongmucuola pluton crystalized at $17.142 \pm 0.014/0.014/0.023$ Ma (uncertainties presented as analytical / + tracer / + decay constant uncertainties), with emplacements of the syn-ore P porphyry and post-ore quartz diorite occurring at $16.009 \pm 0.016/0.017/0.024$ and $15.166 \pm 0.010/0.011/0.020$ Ma, respectively. The Re-Os analysis of multiple independent molybdenite separations from single molybdenite-bearing quartz veins yields sub-per-mil-level analytical precision (<1 ‰), which is comparable with that of modern CA-ID-TIMS U-Pb zircon geochronology. The new Re-Os data indicate that the majority of the metals at Qulong were deposited over a minimum duration of 266 ± 13 thousand years (kyr) between $16.126 \pm 0.008/0.060/0.077$ and $15.860 \pm 0.010/0.058/0.075$ Ma, with the main phase of mineralization being broadly synchronous with the emplacement of the P porphyry. However, our Re-Os data of molybdenite hosted within the Rongmucuola pluton imply that a portion of mineralization also predated the P porphyry, and suggest that the P porphyry is an intermineral porphyry stock, although mineralization cut by P porphyry has not been previously documented or observed in this study. Correlating the Re-Os ages with vein types (A-B-D veins) demonstrates that the mineralization process was cyclical with the presence of at least 3 short-lived (38 ± 11 to 59 ± 10 kyr) mineralization pulses between 16.126 ± 0.008 and 16.050 ± 0.005 Ma, 16.040 ± 0.007 and 15.981 ± 0.007 Ma, and $\sim 15.981 \pm 0.007$ and 15.860 ± 0.010 Ma. Coupling the Re-Os molybdenite ages and quartz (co-precipitated with the dated molybdenite) fluid inclusion data suggests that the cooling history was also cyclic,

and implies a rapid cooling rate during the entire mineralization process (0.55 ± 0.11 °C/kyr), with much faster cooling rates (1.19 ± 0.82 - 1.27 ± 0.53 °C/kyr) for the individual mineralization pulses. The cyclic and rapid cooling process requires additional cooling mechanism rather than the inefficient conduction, which we attribute to meteoric water circulation.

The presence of mineralization predating the intermineral P porphyry stock and the absence of evidence of an early porphyry stock at Qulong suggest that mineralization potentially can take place without contemporaneous magmatism at mineralization levels. As a result, dating magmatic events may not necessarily bracket the entire mineralization duration of a porphyry system. This highlights the importance of dating ore minerals to fully reveal the magma-hydrothermal process. In addition, the absence of contemporaneous magmatism during mineralization have broad implications for the classification of porphyry copper deposits and mineral exploration. The timescales of mineralization cycles constrained here via direct dating of ore minerals (tens of kyr) are comparable with those recently proposed through high-precision U-Pb zircon dating, diffusion modelling and numerical simulation. We propose that the cyclic mineralization pulses are linked with the periodic release of volatile from the lower crustal magma chamber, and such cyclic processes are common for porphyry copper systems worldwide. As such episodic/cyclic metal-enrichment potentially is one of the controlling factors of porphyry copper ore formation, and are therefore key to differentiate the formation of economic and sub-economic porphyry deposits.

Finally, direct comparison of molybdenite Re-Os dates from different labs and with the zircon U-Pb system needs to account for the much larger uncertainties from tracer calibration and decay constants, respectively, which therefore loses the necessary resolution to investigate the ore-forming process at the kyr level. As a result, calibration between the

64 two chronometers and using shared tracer solutions and a transparent data reduction platform
65 within the community is required.

1 Introduction

Metals forming porphyry copper deposits are derived the lower crust and transported to the shallow mineralization levels by magmatic fluids via porphyry stocks that act as conduits (Cooke et al., 2014; Richards, 2011; Sillitoe, 2010). Although this model is widely accepted, there is a paucity of detailed, precise and robust timeframes of igneous and hydrothermal systems to test this hypothesis. For example, at what level are mineralization and magmatism contemporaneous? Moreover, the duration of the porphyry mineralization process is poorly constrained, with studies suggesting orders of magnitude variation, from tens of thousands years to several millions of years (Myr) (Chiaradia et al., 2014).

The timescales of ore formation in porphyry copper deposits can be constrained through the dating of pre- and post-ore intrusions. Traditionally, *in-situ* zircon U-Pb dates are used to establish the timeframe of porphyry stocks and constrain the duration of ore formation (Deckart et al., 2012; Sillitoe and Mortensen, 2010). However, limited by the precision (~2 %) of *in-situ* U-Pb zircon analysis (Klötzli et al., 2009; Li et al., 2015; Schaltegger et al., 2015; Schoene, 2014), the conclusions of these studies are controversial (von Quadt et al., 2011). High-precision (per mil level) dating techniques, e.g., CA-ID-TIMS zircon U-Pb geochronology, make it possible to refine the timeframe and timescales of porphyry copper systems (von Quadt et al., 2011). Recent high-precision zircon U-Pb geochronology case studies indicate that the lifetime of porphyry Cu deposits varies from tens to hundreds of kyr, and by inference suggest the presence of multiple magmatic-hydrothermal episodes (Buret et al., 2016; Chelle-Michou et al., 2015; Tapster et al., 2016; von Quadt et al., 2011). The latter is supported by numerical simulation and diffusion modelling, which suggest that the ore-forming event involves multiple short-lived (several tens of kyr) mineralization pulses (Cathles, 1977; Chelle-Michou et al., 2017; Mercer et al., 2015; Weis, 2015; Weis et al., 2012). However, these approaches (U-Pb dating, numerical

simulation and diffusion modelling) are either based on dating porphyry stocks, which do not necessarily bracket the entire mineralization duration, and/or age constraints of silicate minerals, which may not co-precipitate with ore-minerals, or numerical models that do not fully reflect the complexity of a certain porphyry system.

The most straightforward approach to constrain the timing and duration of ore-forming events is directly dating the ore minerals. The ubiquitous distribution of molybdenite in porphyry Cu-Mo deposits and advances in molybdenite Re-Os geochronology permit precise dating of the ore-forming event(s) directly (Spencer et al., 2015; Stein, 2014). High-precision molybdenite Re-Os dating of the El Salvador and El Teniente porphyry Cu-Mo deposits derived a mineralization duration of 0.6 Myr (Zimmerman et al., 2014), and presence of multiple short-lived (<100 kyr) mineralization pulses over 1.7 Myr (Spencer et al., 2015), respectively. As each complete mineralization pulse comprises petrographically defined veinlets, which are termed as A (earliest), B, D (latest) veins (Gustafson and Hunt, 1975; Sillitoe, 2010), multi-pulsed mineralization events will result in a complex evolution history (i.e., A veins that are younger than D veins). This has been supported by high-precision Re-Os dating of the Los Pelambres Cu-(Mo) deposit, which shows that D veins are ~1 Myr older than B veins (Stein, 2014).

As discussed above, multiple magmatic-hydrothermal/mineralization pulses are evident for deposits with prolonged formation intervals (e.g., several Myr). However, for deposits with shorter formation intervals (e.g., several to tens to hundreds of kyr), which, in some cases, are at the same magnitude as the precision of the dating method, there is an enhanced need to apply high-precision dating to understand the chronology and duration of the ore-forming process. Moreover, due to a lack of deposit-wide crosscutting relationships, it is not clear yet whether these short-lived systems are formed via a single protracted pulse or through multiple short-lived intermittent pulses. In addition, for deposits incrementally

116 formed by several successive mineralization pulses, the timescale of individual pulses
117 remains unknown. The answers for these questions will aid our understanding of metal
118 deposition processes in porphyry copper deposits and shape exploration strategy, e.g., are
119 multiple mineralization pulses necessary to form giant deposits, or is a prolonged
120 mineralization duration essential for economic deposits? Moreover, if multiple magmatic-
121 mineralization events are common in porphyry copper deposits, what is the cooling history of
122 the system? In addition, multiple magmatic-hydrothermal/mineralization events predict
123 thermal resetting for chronometers with low closure temperatures, which need to be
124 considered when interpreting thermochronology dates (e.g., zircon U-Th-He, apatite AFT and
125 mica ^{40}Ar - ^{40}Ar).

126 In this paper, we examine the temporal models (e.g., the temporal relationship
127 between magmatism and mineralization, and the ore-forming processes) of porphyry copper
128 deposits via constraining the ore-forming process of the well-studied Qulong porphyry Cu-
129 Mo deposit by employing CA-ID-TIMS U-Pb zircon and ID-N-TIMS Re-Os molybdenite
130 geochronology with analytical precisions of $\sim 1\%$. Qulong has only one mineralization
131 centre with one main porphyry stock, which makes the deposit a relatively simple and ideal
132 candidate for the research proposed here. The data are used to examine the temporal
133 relationship between magmatism and mineralization, and to propose that one of the main
134 controls of economic porphyry copper systems is episodic/cyclic mineralization events.

136 2 Geological background

137 The Qulong porphyry Cu-Mo deposit is located in the eastern region of the Gangdese
138 magmatic arc (Fig. 1A), which extends along the southern margin of the Lhasa terrane. The
139 Lhasa terrane records the subduction of the Neo-Tethyan oceanic lithosphere and subsequent
140 India-Asia collision (Zhang et al., 2014; Zhu et al., 2015). The eastern part of the Gangdese

magmatic arc is termed the Gangdese Porphyry Copper Belt which contains >20 porphyry copper systems that formed in a collisional or post-collisional (India-Asian) tectonic setting during the Cenozoic (Hou et al., 2009; Wang et al., 2015; Zheng et al., 2015), with the magmas generated by partial melting of a thickened basaltic lower-crust (Hou et al., 2009; Richards, 2015; Wang et al., 2014). Of these porphyry copper systems, eight of them have Cu reserves in excess of 0.5 million tonnes (Mt), with Qulong being the largest both in this belt and China, which hosts ~11 Mt Cu and >0.5 Mt Mo (Hu et al., 2015; Li et al., 2017b; Yang et al., 2009; Zhao et al., 2016).

2.1 Miocene intrusive units at Qulong

The Mid-Miocene Qulong deposit is spatially associated with the Rongmucuola pluton, aplite, P porphyry, X porphyry, two stages of breccia, and quartz diorite units (Fig. 1). The P porphyry and orebody show a spatial association with a north-south striking normal fault system (Fig. 1). The geology of the Qulong system has been described in detail by many previous studies (Hu et al., 2015; Li et al., 2017b; Xiao et al., 2012; Yang et al., 2009; Zhao et al., 2016; Zheng et al., 2004), which we summarise and discuss below. The relative chronology of these units defined by crosscutting relationships is presented in Figure 2A (Hu et al., 2015; Li et al., 2017b; Yang et al., 2009; Zhao et al., 2016).

The Mid-Miocene Rongmucuola pluton is the predominant host lithology to the mineralization of Qulong, which intruded into the Jurassic volcanic (Yeba Formation) and intrusive rocks (dacite-rhyolite porphyry). The pluton has a surface exposure of ~8 km² and a depth of >2 km as constrained by drilling (Fig. 1B-C). The Rongmucuola pluton's composition varies gradually from granodiorite to biotite monzogranite (Fig. 1B) from east to west (Yang et al., 2009; Zhao et al., 2016). Despite this compositional variation, the entire pluton possesses a similar mineralogy (plagioclase, K-feldspar, quartz, amphibole and biotite,

Fig. 3A), however mineralization is only present in the western Rongmucuola pluton (Fig. 1B). The western Rongmucuola pluton is cut by small aplite dikes, the P porphyry, the X porphyry, and a breccia pipe. The aplite hosted by the Rongmucuola pluton has limited distribution in the drill cores and occurs as several to tens of centimetres wide discontinuous fracture-controlled dikes (Li et al., 2017b; Yang et al., 2009; Zhao et al., 2016). The aplite is characterized by intergrowths of fine-grained (~1 mm) anhedral alkali feldspar and quartz with disseminated magnetite and pyrite (Li et al., 2017b; Yang et al., 2009).

The P porphyry, which has an exposure diameter of ~200 m and a depth of >1.8 km as indicated by drilling, was emplaced into the centre of the western Rongmucuola pluton (Fig. 1B-C). No observed (this study) or documented crosscutting relationships between the aplite and the P porphyry are known (Li et al., 2017b; Yang et al., 2009; Zhao et al., 2016). The P porphyry is monzogranitic in composition (plagioclase, quartz, K-feldspar and amphibole and biotite, Fig. 3B) and occurs in the centre (Fig. 1B-C) of the deposit (Hu et al., 2015; Li et al., 2017b; Yang et al., 2009; Zhao et al., 2016). The X porphyry crosscuts both the western Rongmucuola pluton (Fig. 1C) and the P porphyry (Zhao et al., 2016), and has a limited distribution only being present at shallow levels (<200 m) as discontinuous irregular dikes with variable thickness from a few centimetres to 0.5 m (Li et al., 2017b; Yang et al., 2009). The X porphyry possesses a similar composition and texture with that of the P porphyry, with the exception to its biotite content (3-5 % in the X porphyry vs <3 % in the P porphyry, Yang et al., 2009). A magmatic-hydrothermal breccia pipe with a diameter of ~100 m (Fig. 1C) and unknown depth (>500 m) is observed to only crosscut the western Rongmucuola pluton (Li et al., 2017b; Yang et al., 2009; Zhao et al., 2016). The breccia pipe contains two stages of breccia formation, with the first stage breccia comprising clasts (<2 cm) of the mineralized and hydrothermally altered Rongmucuola pluton and the X porphyry, which is crosscut by the second stage breccia, which is characterized by fragments (1 - 10 cm)

of mineralized and hydrothermally altered Rongmucuola pluton (Li et al., 2017b; Yang et al., 2009; Zhao et al., 2016). A cement of a monzogranitic composition, plus mineralized alteration assemblages (e.g., anhydrite, quartz, feldspar, biotite, pyrite and chalcopyrite) is characteristic to both stages of breccia (Yang et al., 2009).

The cessation of magmatism at Qulong is marked by a quartz diorite (plagioclase, quartz and hornblende, Fig. 3C), which intrudes the Rongmucuola pluton (Fig. 1C) as discontinuous dikes with a thickness of 2 - 6 m (Hu et al., 2015; Li et al., 2017b; Yang et al., 2009; Zhao et al., 2016). The quartz diorite exhibits a low degree of alteration as evidenced by the plagioclase phenocrysts. The alteration assemblage consists of calcite-chlorite-sericite and clay minerals (Li et al., 2017b; Yang et al., 2015).

2.2 Alteration and mineralization at Qulong

Mineralization at Qulong is predominately (>80 %) hosted by the western Rongmucuola pluton. Drill core logging indicates that the Cu-Mo metals are directly associated with potassic stage alteration assemblages (80 %), though propylitic and phyllic alteration assemblages also contain Cu-Mo mineralization (Hu et al., 2015; Li et al., 2017b; Yang et al., 2009; Zhao et al., 2016). The potassic stage alteration is ubiquitous in the western Rongmucuola pluton with the most intensive alteration assemblages being spatially associated with the P porphyry and the N-S trending fault system (Li et al., 2017b; Yang et al., 2009). Propylitic alteration assemblages predominately occur in the western Rongmucuola pluton, and overprint potassic alteration assemblages (Yang et al., 2009). Both potassic and propylitic stage alterations are overprinted by pervasive phyllic stage alteration assemblages in the western Rongmucuola pluton (Li et al., 2017b; Yang et al., 2009; Zhao et al., 2016). In the first order, the grades of Cu-Mo metals exhibit concentrically zoned patterns (Fig. 1D-E) around the P porphyry and the N-S trending fault (Yang et al., 2009), although the ore with

the highest grade does decouple from the P porphyry. The decoupling is most evident for the grade of Mo in the orebody, with the highest grade of ore only occurs on the eastern side of the P porphyry (Fig. 1E). Considering the small size, limited and discontinuous distribution of the aplite and the X porphyry, it is currently accepted that the P porphyry is the main fluid conduit at Qulong (Hu et al., 2015; Li et al., 2017b; Yang et al., 2009; Zhao et al., 2016). The ore minerals at Qulong are chalcopyrite and molybdenite with trace amounts of bornite. The ore minerals are predominately hosted by quartz vein assemblages in the western Rongmucuola pluton (Li et al., 2017b; Yang et al., 2009), and to a lesser extent by the Jurassic Yeba Formation. Except for very minor disseminated molybdenite clusters (<1 mm) or quartz veins with very minor molybdenite (equivalent to <0.5 mg), which also exhibit intensive hydrothermal overprint by late stage propylitic and phyllic alteration, no molybdenite-bearing veins with limited overprint and appreciable molybdenite (≥ 10 mg) have been observed in the P porphyry during the course of study. Further, according to previous drill core logging (Hu et al., 2015; Li et al., 2017b; Yang et al., 2009; Zhao et al., 2016) and observation of this study, the P porphyry does not crosscut any mineralization. The quartz veins are classified as A, B and D veins (Fig. 4) based on previous studies (Li et al., 2017b; Yang et al., 2009) and by following the vein terminology/classification of Gustafson and Hunt (1975) and Sillitoe (2010). Representative A, B and D veins observed at Qulong are presented in Figure 4. The A veins are characterized by 0.3 - 0.8 cm wide discontinuous granular quartz veinlets with discontinuous narrow (< 3 mm) K-feldspar selvages, which host disseminated chalcopyrite and molybdenite (Fig. 4A). The B veins are represented by veinlets (0.4 - 2 cm wide) comprising crystalline quartz with a crack-seal texture, and possess irregularly distributed K-feldspar selvage, and predominantly host molybdenite and chalcopyrite along the vein margin (Fig. 4B). The D quartz veins (0.5 - 6 cm) host euhedral

pyrite, with sericite and anhydrite (0.1 and 1.5 cm) selvages (Fig. 4D), and minor disseminated chalcopyrite and molybdenite.

The relative timing relationships between different vein types, e.g., barren A vein cut by later mineralized A vein and/or B vein, have been previously documented (Li et al., 2017b; Yang et al., 2009) and also observed in this study (Fig. 4E-F). However, importantly to avoid any potential mixing of different generations of mineralization and therefore to yield robust molybdenite Re-Os geochronology, this study focused on veins without cross-cutting relationships by later veins and that show the least evidence of overprinting (e.g., Fig. 4A, B, D).

2.3 Previous Geochronology

The Qulong deposit has been studied extensively with the principal goal to establish the timing of magmatism, mineralization and timeframe of cooling (Hou et al., 2004; Hu et al., 2015; Li et al., 2017b; Wang et al., 2006; Yang et al., 2009; Yang et al., 2015; Zhao et al., 2016; Zheng et al., 2004) and references therein). These studies established the timeframe of the Qulong porphyry system (Fig. 2A) via LA-ICPMS and SHRIMP/SIMS (U-Pb zircon, appendix Table A1) and ID-ICPMS (Re-Os molybdenite, appendix Table A2). Samples from the western Rongmucuola pluton dated by *in-situ* zircon U-Pb yield variable weighted mean $^{206}\text{Pb}/^{238}\text{U}$ dates between 17.6 ± 0.4 Ma and 16.2 ± 0.3 Ma, with dates from the P porphyry varying from 17.58 ± 0.74 Ma to 16.2 ± 0.4 Ma. The X porphyry has a mean $^{206}\text{Pb}/^{238}\text{U}$ date of 15.9 ± 0.4 Ma and post-ore quartz diorite yield mean $^{206}\text{Pb}/^{238}\text{U}$ dates of 15.7 ± 0.2 and 15.3 ± 0.3 Ma. Molybdenite hosted by the Rongmucuola pluton yield variable dates ranging from 16.85 ± 0.19 to 15.36 ± 0.21 Ma. These prior studies provide a basic framework for the formation time of Qulong. However, the emplacement ages of the intrusions constrained by *in-situ* U-Pb zircon techniques and the mineralization ages determined by ID-ICP-MS

molybdenite Re-Os methodology have significant uncertainties (1.3 - 4.2 % and 1.1 - 12.2 %, respectively), which equate to absolute uncertainties of 0.2 - 0.7 and 0.2 - 1.9 Myr, respectively, for the U-Pb and Re-Os dates of the ~16 Ma porphyry system. In order to evaluate the dates of the same intrusion from different studies, the mean and 2 standard deviation of zircon U-Pb $^{206}\text{Pb}/^{238}\text{U}$ data from different studies with different dating techniques are presented in **Figure 2B**. The reason for using the mean and 2 standard deviation, rather than weighted mean, is that dates from different studies are not equivalent and cannot be regarded as one population. The significant variations demonstrated in Figure 2B either reflect the complexity of ages (e.g., complex magmatic evolution history) the zircon grains record (Chelle-Michou et al., 2014), and/or unaccounted analytical bias inherited in micro-beam analysis (Li et al., 2015). As demonstrated previously (von Quadt et al., 2011), the uncertainties of these data are mostly greater than the timescales proposed for the ore formation processes (Chiaradia et al., 2014). Therefore, these dates cannot be used to precisely define the durations of the magmatic and mineralization event(s) and further develop models for ore formation (Schaltegger et al., 2015).

3 Samples and analytical methods

To provide robust and precise time constraints for the Qulong porphyry Cu-Mo system, high-precision CA-ID-TIMS zircon U-Pb geochronology and ID-N-TIMS molybdenite Re-Os dating are employed. Representative samples with limited alteration of the western Rongmucuola pluton, P porphyry, and the quartz diorite (**Fig. 3**) were collected from drill core to conduct U-Pb zircon dating. The X porphyry has been exhausted by previous studies in the available drill core we studied, as such the X porphyry was not available for CA-ID-TIMS zircon U-Pb analysis for this study. A previous attempt to date the

aplite by SIMS zircon U-Pb analysis demonstrated that the aplite only contains inherited grains (Li et al., 2017b), and in this case the aplite is not further investigated by CA-ID-TIMS.

The sample from the Rongmucuola pluton (1605-296, Fig. 3A) used for U-Pb dating exhibits a low degree of hydrothermal alteration and mineralization, as evidenced by the rims of the biotite and plagioclase, which are altered to chlorite and sericite, with the groundmass possessing minor disseminated pyrite. The P porphyry sample (001-550, Fig. 3B) used for U-Pb dating is extensively hydrothermally altered and overprinted by multiple stages of alteration assemblages. The quartz phenocrysts exhibit an embayed morphology and K-feldspar shows partial replacement by sericite. In addition, the groundmass displays different degrees of hypogene alteration. For example, plagioclase and biotite either exhibit complete or partial destruction with alteration to sericite/clay and chlorite, respectively. The quartz diorite sample (1605-81, Fig. 3C) used for U-Pb dating only exhibits minor alteration, as represented by the rims of the plagioclase phenocrysts which are altered to calcite-chlorite-sericite and clay minerals.

To yield robust molybdenite Re-Os geochronology, e.g., avoid any potential disturbance of Re-Os by overprinting and mixing different stages of mineralization, veins without intersections and exhibiting the least evidence of overprint (e.g., Fig. 4A, B, D) were selected for molybdenite Re-Os geochronology. Three A veins, 7 B veins and 3 D veins, were selected to conduct high precision ID-N-TIMS Re-Os molybdenite geochronology. All of the veins used for Re-Os molybdenite geochronology are hosted by the western Rongmucuola pluton, with the exception of one vein (sample 313-145), which is hosted by an aplite dike. The dated molybdenite-bearing veins are identical to those used previously for a fluid inclusion study (Li et al., 2017b), and therefore permit coupling vein formation ages and temperatures (see discussion). The sample number of studied igneous rocks and molybdenite-

bearing veins is made up by the drill core number and sample depth in meters. Locations of drill are marked in Figure 1B.

3.1 CA-ID-TIMS zircon U-Pb

The methods for U-Pb geochronology are the same as previously documented by (Tapster et al., 2016). Mineral separation was carried out at the NERC Isotope Geosciences laboratory (NIGL), British Geological Survey (BGS), Nottingham, UK. Zircons were isolated from ~1.5 kg drill core samples. After washing, samples were jaw crushed, disc milled and sieved (<355 μm mesh). Heavy minerals were concentrated using a Rogers table, then a Frantz electromagnetic separator and finally by standard heavy liquid (diiodomethane) concentration. Zircon grains from the concentrated materials were then handpicked under a binocular microscope and mounted in epoxy, and then polished with a 0.25 μm diamond paste and finished at near-equatorial sections to yield the best internal exposure of the zircon grains.

The mounts were coated with carbon for CL imaging (Li et al., 2017a), and zircon grains with least inclusions and no indication of inheritance cores (Fig. 3) were removed from the mounts and then individually thermally annealed in quartz crucibles at 900 °C for ~60 hours as part of the chemical abrasion process (Mattinson, 2005). The zircons were then individually ultrasonically cleaned in warm 4N HNO₃, and further rinsed with 4N HNO₃ and ultrapure acetone. The chemical abrasion was continued by loading the zircons individually into 300 μl FEP Teflon microcapsules with 200 μl 29 N HF with trace 4N HNO₃. The microcapsules were placed in a self-sealing ParrTM vessel at ~180 °C for 12 hours (Mattinson, 2005). The leachate was removed, with the zircon fractions being rinsed in 4N HNO₃, fluxed in 6N HCl at ~80 °C for several hours, and further rinsed in 4N HNO₃ and ultrapure water. The leached zircons were spiked with the mixed ²⁰²Pb-²⁰⁵Pb-²³³U-²³⁵U EARTHTIME tracer

solutions (ET2535, Condon et al., 2015; McLean et al., 2015) before dissolution with ~120 μl of 29N HF and trace HNO_3 in ParrTM vessels at ~220 °C for 60 hours. Solutions of the equilibrated tracer and dissolved zircon were evaporated and re-dissolved in ParrTM vessels overnight in 200 μl 3N HCl at 180 °C. Uranium and Pb were separated by standard HCl-based anion-exchange chemistry (Krogh, 1973) and evaporated to dryness with 2 μl of 0.05N H_3PO_4 .

Uranium and Pb were loaded together on a single zone-refined Re filament in a silica gel-phosphoric acid matrix (Gerstenberger and Haase, 1997). Isotope ratios were measured using a Thermo-Electron Triton Thermal Ionization Mass-Spectrometer. Uranium was measured as an oxide (UO_2) in static Faraday mode on Faraday detectors equipped with 10^{12} Ω resistors for intensities greater than 4 mV or peak-hopping mode on a SEM detector for low-U samples. The isobaric interferences are corrected using a $^{18}\text{O}/^{16}\text{O}$ value of 0.00205 (Condon et al., 2015). Lead isotopic compositions were measured by peak-hopping mode on a secondary electron multiplier detector (SEM). Linearity characterization and dead time corrections (Pb = 24.5 ns; U = 22 ns) for SEM measurements were made from long-term monitoring of the NBS 982, NBS 981 and U 500 standards.

Measured U and Pb isotopic data were processed using the TRIPOLI software package (Bowring et al., 2011). Data reduction, error propagation, data calculation and presentation were conducted using ET_Redux and related algorithms (McLean et al., 2011). Mass bias for Pb isotope measurement was corrected with real-time $^{202}\text{Pb}/^{205}\text{Pb}$ ratios (Condon et al., 2015; McLean et al., 2015). The U mass fractionation was calculated in real-time based on the isotopic composition of the EARTHTIME tracer solutions. Decay constants used here are from Cheng et al. (2000) for ^{230}Th , Jaffey et al. (1971) for ^{238}U and ^{235}U , with the value of $^{238}\text{U}/^{235}\text{U}$ from Hiess et al. (2012).

All common Pb (Pbc) was attributed to an isotopic composition of the NIGL laboratory blank of $^{206}\text{Pb}/^{204}\text{Pb} = 18.099 \pm 3.02 \%$, $^{207}\text{Pb}/^{204}\text{Pb} = 15.545 \pm 1.758 \%$ and $^{208}\text{Pb}/^{204}\text{Pb} = 37.824 \pm 2.814 \%$ (2σ uncertainties) for the analytical period. For most zircon grains, the radiogenic Pb are high compared with common Pb (with a ratio >5 in most cases), showing that the results are insensitive to the common Pb corrections (Table 1). The U blanks were assigned a value of 0.10 ± 0.02 pg (2σ) based upon total procedural blanks.

The preferential inclusion of ^{238}U and exclusion of ^{230}Th during zircon crystallization (Schärer, 1984), and thus eventual deficit in ^{206}Pb (younger apparent dates), was accounted via Th disequilibrium correction. For corrections, the Th/U values of the bulk samples were used to represent the Th/U value of the melt at the time of zircon crystallization (Schärer, 1984).

The Th/U values of the Rongmucuola pluton, the P porphyry and the quartz diorite are 4.0, 3.6 and 5.0, respectively (Yang et al., 2009). These values were used with an uncertainty of ± 2 (2σ) to correct the initial ^{230}Th disequilibrium. However, the Th/U values of individual zircons may vary due to fractional crystallization, partition coefficients, temperature and oxidation state (Burnham and Berry, 2012; Luo and Ayers, 2009; Rubatto and Hermann, 2007). To account for all these complexities, we further investigated the sensitivity of the ^{230}Th correction by varying the Th/U values within geologically feasible values between 1 and 7 (Fig. 5). As demonstrated by using the youngest group comprising 3 zircon dates from the P porphyry (see below for detailed discussion), the weighted average of the youngest group varied by less than 40 kyr over the range of Th/U values between 2 and 7 (Fig. 5A), and the statistically acceptable MSWD values (e.g., <1.5 , Fig. 5B) were maintained throughout. In addition, within uncertainties, the weighted average from our preferred solution (using the bulk sample's Th/U value for correction) overlapped with those corrected from Th/U values of 2 - 7 (Fig. 5A). However, when magmatic Th/U value

approaches unity ($\text{Th}/\text{U} = 1$), a significantly younger date was determined. Given that the Th/U values of the Rongmucuola pluton, the P porphyry and the quartz diorite are 4.0, 3.6 and 5.0, respectively (Yang et al., 2009), we consider that correcting for initial ^{230}Th disequilibrium using a $\text{Th}/\text{U} \leq 1$ is a geologically unreasonable assumption. Therefore, using Th/U values (± 2 , 2σ) of the bulk samples is a reasonable and valid approach.

3.2 ID-NTIMS molybdenite Re-Os

The molybdenite separation and Re-Os dating methods are adopted from previous studies (Lawley and Selby, 2012; Selby and Creaser, 2001). Molybdenite-bearing (0.3 - 3 mm grain size) quartz veins were selected based on previous petrography and fluid inclusion study (Li et al., 2017b), and then cut into several parts depending on molybdenite abundance (Fig. 6). The fractions were then individually crushed by an agate pestle to 10 mesh (~ 2 mm) and then handpicked under a binocular microscope to remove non-molybdenite-bearing phases and to examine the genetic association between quartz and molybdenite. The pre-purified materials (quartz-bearing molybdenite) of individual separations were loaded into Teflon beakers with 10 ml 32 N HF to dissolve quartz at room temperature overnight (Lawley and Selby, 2012). The HF purification step was repeated until most of the quartz fractions were dissolved, e.g., most of the molybdenites are liberated. The molybdenites were then rinsed with MQ three times and further rinsed with ethanol, and then dried at $\sim 35^\circ\text{C}$. The concentrated molybdenite aliquots were further purified (removal of any pyrite/chalcopyrite and undissolved silicate phases) by hand under a binocular microscope. The purity of the mineral separate was estimated to be better than 95 %.

This approach, dating multiple independent molybdenite separations from a single vein (Fig. 6A-B), offers the opportunity to check the consistency and closed system behavior of the Re-Os system within the vein and ultimately verify the accuracy of the dates as further

discussed below. In addition, similar to that of zircon U-Pb geochronology, this approach permits calculating a weighted average of dates from the same vein and statistically reduces the effect of the analytical uncertainties.

For molybdenite digestion, a known amount of molybdenite (typically >20 mg) and tracer solution (^{185}Re plus isotopically normal Os, Selby and Creaser, 2001) was loaded into a Carius tube (Shirey and Walker, 1995) with 3 ml 15.5 N HCl and 6 ml 16 N HNO_3 , sealed and placed in steel jackets. The Carius tube bearing jackets were placed in an oven to digest at 220 °C for ~24 hours, which permitted the achievement of both rhenium and osmium isotopic equilibrium between the tracer and sample (Selby and Creaser, 2001). Once cooled to room temperature, the outsides of the tubes were carefully rinsed by MQ to remove any particles and then dried. The bottom parts of the Carius tubes were frozen in a mixture of dry ice and ethanol and then opened from the top by a $\text{H}_2\text{-O}_2$ flame in a fume hood. Osmium was isolated from the acid medium using solvent extraction method (CHCl_3 ; 3 x 3 mL) at room temperature (Shen et al., 1996), and then back extracted into HBr (Cohen and Waters, 1996) on a rocker overnight. The Os-bearing HBr solution was dried with the Os further purified by micro-distillation (Birck et al., 1997; Roy-Barman, 1993). After Os extraction, the Re-bearing acid medium was dried and then separated by NaOH-acetone solvent extraction (Cumming et al., 2013; Matthews and Riley, 1970). The Re was further purified via modified standard anion column chromatography (Morgan et al., 1991).

Rhenium and Os were loaded onto outgassed Ni and Pt filaments, respectively. The isotopic compositions of Re and Os were measured by negative thermal ionization mass spectrometry (N-TIMS) as ReO_4^- and OsO_3^- , respectively (Creaser et al., 1991; Völkening et al., 1991). The mass spectrometer analysis was conducted on a Thermo Scientific TRITON mass spectrometer at Durham University, with Re and Os isotopic compositions measured using static Faraday cups collection mode. The measured Re and Os isotopic compositions

were corrected using a $^{18}\text{O}/^{16}\text{O}$ and $^{17}\text{O}/^{16}\text{O}$ value of 0.002045 and 0.001113 (Nier, 1950). The isotopic composition of Re was corrected for instrumental fractionation by fractionation factors defined by the differences between standard Re analyses and the value of Gramlich et al. (1973; $^{185}\text{Re}/^{187}\text{Re} = 0.59738$) before and after the sample Re measurements. The Os mass fractionation was monitored in real-time by monitoring the Os isotopic composition of the tracer and corrected using a $^{192}\text{Os}/^{188}\text{Os}$ of 3.08761. The uncertainties of sample Re and Os isotopic composition measurements, tracer calibration, sample and tracer weighting, reproducibility of Re and Os isotope standards, as well as blank abundances and isotopic compositions during the course of study were all propagated. During this study, the Re and Os blanks were 2 pg and 0.5 pg, respectively, with a $^{187}\text{Os}/^{188}\text{Os}$ value of 0.24 ± 0.01 ($n = 6$, 2σ). The high Re and Os abundances (Table 2) in these samples in comparison to the blanks result in a negligible blank correction to the final date ($<0.035\%$).

The molybdenite Re-Os model date was calculated using the equation $t = \ln(^{187}\text{Os}/^{187}\text{Re} + 1)/\lambda$, in which λ is the decay constant (Smoliar et al., 1996). Using the ^{187}Re decay constant of (Selby et al., 2007) yield model dates that are ~ 0.008 Ma younger than those calculated with ^{187}Re decay constant of (Smoliar et al., 1996). This small systematic discrepancy is a level similar to the analytical uncertainty and the model dates calculated with two ^{187}Re decay constants overlap within uncertainties. Therefore, we consider that using either ^{187}Re decay constants does not impact the interpretation of the final date.

To evaluate the accuracy and reproducibility of the molybdenite Re-Os analytical approach, the Henderson molybdenite reference material (RM8599) was run during the course of this study. Nine analyses of RM8599 yield a weighted mean of 27.695 ± 0.038 (2σ , MSWD = 0.53, Fig. 6C), which is in good agreement with the recommended value 27.66 ± 0.10 Ma (Markey et al., 2007; Zimmerman et al., 2014), and previous analysis at Durham (Lawley and Selby, 2012).

A further consideration, although negligible, is the presence of trace amounts of common ^{187}Os in the molybdenite (Selby and Creaser, 2001; Stein, 2014; Stein et al., 2001), which is not accounted for by the analytical method using a tracer solution with a normal Os isotopic composition (Markey et al., 2007; Selby and Creaser, 2001). However, the levels of common ^{187}Os in most published molybdenite is $<\sim 23$ ppt, and typically < 6 ppt (Spencer et al., 2015; Stein, 2014; Stein et al., 2001; Zimmerman et al., 2014). Therefore, this level of common ^{187}Os will only alter the model dates of the studied samples by 1-10 kyr (33 of the 42 dates < 3 kyr). Further, our approach of obtaining multiple independent dates from a single vein (Fig. 6A-B) is an independent test for the consistency of the Re-Os systematics along the vein. The reproducible dates (Table 2) from the same vein verifies the accuracy of the model dates, and support the negligible presence of common ^{187}Os in molybdenite since a single vein can be regarded as a specific geological event (Stein, 2006). Finally, as other tracers (e.g., ^{190}Os - ^{188}Os tracer) are calibrated against the common Os solution/tracer (Markey et al., 2007), their precision will never be better than that of the common Os tracer, and as a result dates obtained using a common Os tracer, will, in principle, have smaller uncertainties inherited from tracer calibration.

3.3 Uncertainties of duration and cooling rates

As this study is utilizing high-precision dates to constrain the ore-forming process, e.g., the duration and cooling rates, it is particularly important to evaluate the uncertainties associated with the dates. For durations calculated from the same radio-isotopic system, e.g., Re-Os or U-Pb, either analytical uncertainty or analytical + tracer calibration uncertainties are considered for dates using the same tracer or different tracer, respectively. For example, when calculating the duration of mineralization (Re-Os system), or the temporal gap between the emplacement of the Rongmucuola pluton and the P porphyry (U-Pb system), only analytical

uncertainties needs to accounted. Considering that molybdenite Re-Os and zircon U-Pb dates are ‘independent’ chronometers, the uncertainty related to calibration of both systems must be considered (i.e., tracer calibration and decay constants) when comparing the two chronometers to derive a geological inference.

The uncertainties of the duration or rates are propagated using a Monto Carlo simulation. When calculating the uncertainties of the cooling rates, in addition to considering the analytical uncertainties of the Re-Os dates, the uncertainty in the trapping temperatures of quartz hosted fluid inclusions are used (± 20 °C) (Li et al., 2017b).

4 Results

The uncertainties of the U-Pb and Re-Os dates are presented as $\pm x/y/z$ (analytical uncertainty /+tracer calibration /+decay constant uncertainties) in **Figures 7 and 8 (Tables 1-2)**, respectively.

4.1 Zircon U-Pb geochronology

All the analysed zircon grains from the Rongmucuola pluton, with the exception of two grains, yielded concordant $^{206}\text{Pb}/^{238}\text{U}$ and $^{207}\text{Pb}/^{235}\text{U}$ dates (Fig. 7A).

The 8 zircons from the western Rongmucuola pluton yielded $^{206}\text{Pb}/^{238}\text{U}$ dates of 17.975 - 17.057 Ma (Fig. 7B) with $\text{Th}/\text{U}_{\text{zircon}}$ values of 0.47 - 0.59 (Table 1). The youngest date obtained from a single analysis is 17.057 Ma, but this date could not be reproduced by other zircon grains. A weighted mean, $17.142 \pm 0.014/0.014/0.023$ Ma, was calculated from the youngest cluster of dates that yielded a statistically acceptable population ($\text{MSWD} = 1.12$; $n = 3$).

Seven analyses from the P porphyry yielded $^{206}\text{Pb}/^{238}\text{U}$ dates between 16.115 and 15.998 Ma (**Fig. 7B**), and the youngest cluster of dates gives a weighted mean of $16.009 \pm$

0.016/0.017/0.024 (MSWD = 0.90; n = 3) with Th/U_{zircon} values of 0.92 - 1.11 (Table 1). This group included two fragments of a single elongate prismatic zircon grain (z4A and z4B, Fig. 3D) which yielded indistinguishable dates.

Seven zircons from the quartz diorite yield ²⁰⁶Pb/²³⁸U dates of 15.189 - 15.116 Ma (Fig. 7B) with 6 yielding a weighted mean of 15.166 ± 0.010/0.011/0.020 (MSWD = 1.67).

4.2 Molybdenite Re-Os geochronology

For the 13 molybdenite-bearing veins, multiple (2 - 7) individual molybdenite separates (e.g., Fig. 6) were obtained for each vein, except for 3 veins which only yielded one separate each as a result of a low concentration of molybdenite. In total 42 analyses were conducted, of which six of them were reprocessed after Li et al. (2017b) either through re-analysis of the purified Re fraction or analysis a new aliquot of the identical mineral separate. Overall, the Re and ¹⁸⁷Os abundances of these samples range from 60 to 504 ppm, and from 10 to 85 ppb, respectively (Table 2).

The weighted mean dates were calculated for each vein, with the exception of the three veins with only one analysis. The weighted mean dates or model dates (three samples with one analysis) for these veins span from 16.126 ± 0.008/0.060/0.077 (n = 3, MSWD = 1.9) to 15.860 ± 0.010/0.058/0.075 Ma (n = 2, MSWD = 0.021) and do not form a single statistic population (Fig. 8). Dates of A, B and D veins vary from 16.126 ± 0.008/0.060/0.077 (n = 3, MSWD = 1.9) to 16.040 ± 0.007/0.058/0.075 Ma (n = 4, MSWD = 0.69), from 16.107 ± 0.015/0.065/0.082 (n = 1) to 15.939 ± 0.006/0.058/0.075 Ma (n = 4, MSWD = 1.6), and from 16.088 ± 0.007/0.059/0.076 (n = 3, MSWD = 1.6) to 15.860 ± 0.010/0.058/0.075 Ma (n = 2, MSWD = 0.021), respectively. No relationship is observed between dates and vein types, although all A veins are older than 16.040 ± 0.007/0.058/0.075 Ma (Fig. 8).

5 Discussion

5.1 A refined chronology of the Qulong porphyry system

Regarding the emplacement ages of the dated igneous units, our preferred interpretation is the weighted averages calculated from the youngest groups of $^{206}\text{Pb}/^{238}\text{U}$ dates. For the Rongmucuola pluton, the youngest date cannot be reproduced by other grains. To avoid biasing the emplacement age to a younger date, which could potential be related to lead loss, we consider the weighted average of the youngest cluster, $17.142 \pm 0.014/0.014/0.023$ (MSWD = 1.12; $n = 3$), as our preferred estimate of the emplacement age of the western Rongmucuola pluton (Fig. 7).

The youngest cluster of zircon grains from the P porphyry comprises two fragments of a single elongate prismatic zircon grain (z4A and z4B, Fig. 3D), therefore supporting the hypothesis that the lead loss domains, if occurred, was efficiently removed by the chemical abrasion process. As such, we consider the weighted mean, $16.009 \pm 0.016/0.017/0.024$ (MSWD = 0.90; $n = 3$), as the best estimate of the emplacement age of the P porphyry.

The best estimated emplacement age of the quartz diorite is $15.166 \pm 0.010/0.011/0.020$ (MSWD = 1.67, $n = 6$), represented by the weighted average calculated from 6 of the 7 zircon Miocene dates (Fig. 7B).

The oldest discordant zircon from the Rongmucuola pluton is interpreted as a result of the incorporation of xenocrystic cores from an older magmatic source. A similar scenario is preferred to explain the ~ 36.267 Ma grain from the quartz diorite (Table 1). The older dates from each pluton are interpreted as a mixture of two age domains (Chelle-Michou et al., 2014), e.g., in addition to the zircon rims formed during the emplacement of the intrusions, the zircons also contain xenocrystic cores, or represent a protracted zircon crystallisation history in an upper crustal magma chamber, and are not discussed further.

As discussed above, our new CA-ID-TIMS U-Pb zircon ages provided here agree with the relative chronology based on field observations (Fig. 2A) and timeframe determined via *in-situ* U-Pb zircon techniques (Fig. 2B), but at a much higher temporal resolution (~0.1 %).

Field relationships show that the Rongmucuola pluton and the quartz diorite are pre-ore and post-ore without further evidence of Miocene magmatism outside this interval (Hu et al., 2015; Li et al., 2017b; Yang et al., 2009; Yang et al., 2015; Zhao et al., 2016). In this regard, the U-Pb ages of the Rongmucuola pluton and the quartz diorite constrain the duration of mineralization-related magmatism at Qulong to 1.976 ± 0.017 Myr. The aplite is observed only in the Rongmucuola pluton without direct crosscutting relationship with both the P and X porphyries (Hu et al., 2015; Li et al., 2017b; Yang et al., 2009; Zhao et al., 2016), and previous SIMS U-Pb zircon geochronology showed only evidence of inheritance (Li et al., 2017b). The minimum emplacement age of the aplite is estimated as 16.126 ± 0.077 Ma (including all sources of uncertainty, e.g., analytical uncertainty /+tracer calibration /+decay constant uncertainties) based on a Re-Os molybdenite date from an A-type quartz-vein hosted by the aplite (sample 313-145, discussed below). Given the emplacement age of the P porphyry is 16.009 ± 0.024 Ma (with all uncertainties), the aplite predates the P porphyry and is at least 0.117 ± 0.081 Myr older.

For molybdenite Re-Os dates, given the similar morphology of molybdenite grains and alteration assemblages within a vein (e.g., Fig. 4), we assume that molybdenite grains in each vein formed at the same time. This assumption, in part, has been supported by the fact that model ages of multiple analyses of each vein (except 1605-33) overlap within uncertainty. For veins with multiple analyses, when the MSWD is acceptable for the number of analyses (Wendt and Carl, 1991), the weighted means are interpreted as molybdenite crystallization ages. By inference, e.g., close spatial association between molybdenite and the

gangue minerals, quartz-bearing fluid inclusions with opaque minerals (Li et al., 2017b), we suggest that molybdenite crystalized at the same time as the gangue minerals, and therefore can be used to represent the vein-formation ages. For 3 veins with one analysis, given the confidence of data reproducibility from multiple analyses of the single vein, the model ages were interpreted as vein formation ages. However, an exception is sample 1605-33, which gives a MSWD of 5 (Fig. 8) and is interpreted to reflect the presence of multiple generations of molybdenite, which nonetheless are not recognized petrographically. As such, the mean calculated from the youngest two analyses is interpreted as the best estimated formation age of that vein.

The Re-Os ages of this study overlap with the majority of the dates from previous studies within uncertainties (Fig. 2B). However, the Re-Os dates of this study are considerably more precise ($\sim 0.1\%$, Fig. 7B) and suggest that the majority of the mineralization occurred between $16.126 \pm 0.008/0.060/0.077$ and $15.860 \pm 0.010/0.058/0.075$ Ma with a duration of $\sim 266 \pm 13$ kyr. This duration is a minimum estimate as there is no geological evidence to exclude the presence of mineralization beyond this interval, and observations at Qulong suggest that Cu mineralization as whole is earlier than the Mo ore. However, we consider that this duration is reasonable as it has been independently shown that, with an average magma flux (pluton filling rate) of $0.01 \text{ km}^3/\text{yr}$, a few tens of million tons of Cu, comparable to the amount of Cu at Qulong, can be accumulated within 200 - 300 kyrs (Chelle-Michou et al., 2017).

The Re-Os dates from previous studies (Fig. 2B and appendix Table A2) have appreciable uncertainties of 1.3 - 12.1 %, which we attribute to analytical challenges associated with initial Re-Os studies, e.g., imprecise determinations of the stoichiometry of Os salts used for tracer calibration (Yin et al., 2001), poor external reproducibility of ICP-MS analysis (Stein, 2014) potentially caused by memory effects of Os and unstabilized ion signal

in the long term, and potential bias between labs (e.g., tracer calibration, data reduction). Given dates of the RM8599 reference materials measured during the course of study agree with the recommended value (Fig. 6C), and the agreement between molybdenite Re-Os and zircon U-Pb chronometers from a preliminary cross-calibration (Selby et al., 2007) with the same Re-Os tracer used in this study, we suggest that, to the best of our knowledge and effort, the molybdenite Re-Os ages from this study are the best estimates of molybdenite crystallization ages at Qulong. For future molybdenite Re-Os geochronology study, we reiterate that measuring and reporting the age values of RM8599 reference materials is essential, coupled with the analysis of a suitable sized aliquant of a mineral separate (e.g., Selby and Creaser, 2004; Stein et al., 2003), and employ the multiple-analysis from a single vein approach proposed here.

5.2 Integrating magmatic and hydrothermal timescales

At Qulong, field observations demonstrate a relatively close spatial association (Fig. 1D-E) between the P porphyry and high-grade Cu ore (Yang et al., 2009; Zheng et al., 2004). In addition, the aplite and X porphyry are very small in size and only distribute discontinuous. Further, there is no other porphyry stocks within 2 km as demonstrated by extensive drilling. Therefore, the P porphyry is regarded as the only observed porphyry stock that can act as a conduit (Hu et al., 2015; Li et al., 2017b; Yang et al., 2009; Zhao et al., 2016). However, this scenario has not been tested due to a lack of cross-cutting relationships at the deposit level. Testing this scenario is possible by dating the P porphyry and mineralization at Qulong with high accuracy and precision, and the null hypothesis is that the porphyry stock is expected to be older than the mineralization.

Considering the emplacement age of the P porphyry is 16.009 ± 0.024 Ma (with all uncertainties at the 2σ level, Fig. 7), 13 of the 16 published molybdenite Re-Os ages overlap

with this emplacement age, while the remaining 3 are older (including all sources of uncertainty, e.g., analytical uncertainty /+tracer calibration /+decay constant uncertainties). The three Re-Os dates that are older than the P porphyry agree with the field observations that all mineralization at Qulong postdate the Rongmucuola pluton and predate the quartz diorite (Fig. 2A). For our molybdenite Re-Os dates, only sample 313-145, which is hosted by the aplite, is 0.117 ± 0.081 older than the P porphyry, with other 11 samples that overlap within uncertainties, and the remaining 1 sample that is nominally younger (Fig. 8).

Excluding analytical issues, the presence of Re-Os dates from this study that predate the P porphyry implies that mineralization did occur before the emplacement of the P porphyry. As mentioned above, the aplite is unlikely to be a conduit given its exceptional small volume (with a width of 0.05 - 2 m) and discontinuous distribution. Together with the absence of other documented/observed porphyry stocks that predate the P porphyry, the most likely scenario is that the P porphyry is an intermineral porphyry stock and potentially a part of the mineralization (e.g., the one yielding ages that predates the P porphyry) was deposited before the emplacement of the P porphyry. This scenario is arguably supported by the observation that the highest grade of Mo ore does not occur within the P porphyry (Fig. 1D-E) (Yang et al., 2009), as intermineral porphyry stocks commonly result in low-grade cores in porphyry deposits (Sillitoe, 2000). The decoupling between shallow magmatism and volatile transportation thus makes it unlikely that all metals were transported by the P porphyry stock at Qulong. However, we reiterate that such a scenario is the most plausible one based on the available data. Further detailed mapping (crosscutting relationships, alteration) could confirm this hypothesis.

5.3 Cyclical mineralization pulses and their timescales

The veins in each mineralization pulse of porphyry copper deposits are classified as A, B and D veins (Fig. 3). The temporal succession of these veins records a progressive change in the fluid nature, e.g., temperature, pH and/or oxygen fugacity, and is widely used to trace fluid evolution processes (Gustafson and Hunt, 1975; Sillitoe, 2010). Given the timescale of hydrothermal activity that can be sustained by a single magmatic episode is limited to several tens of kyr (Buret et al., 2016; Cathles et al., 1997; Chelle-Michou et al., 2015; Mercer et al., 2015; Tapster et al., 2016; Weis et al., 2012), porphyry deposits which show prolonged duration (e.g., several Myr, Chiaradia et al., 2014) clearly imply multiple mineralization pulses, as supported by the presence of repetitive A-B-D veins from field observations and high precision dating (Sillitoe, 2010; Spencer et al., 2015; Stein, 2014). However, it is still not clear whether multiple mineralization pulses are only present in some deposits with prolonged duration, or if they are common in porphyry copper deposits in general. Also questionable is the role of multiple pulses for the formation of economic deposits.

Our geochronological data suggest that the mineralization process at Qulong was likely discontinuous during the 266 ± 13 kyr interval (Fig. 8), and characterized by the presence of at least two A-B-D cycles and one incomplete (B-D) cycle. Our Re-Os data constrain the lifetime of the two short-lived A-B-D cycles to 38 ± 11 and 59 ± 10 kyr with a gap of 48 ± 10 kyr between them. The timescales of mineralization cycles constrained here (tens of kyr) by direct dating of ore minerals are comparable with those recently proposed through high-precision dating (Buret et al., 2016; Chelle-Michou et al., 2015; Tapster et al., 2016), titanium diffusion in quartz (Mercer et al., 2015) and numerical modeling (Chelle-Michou et al., 2017; Weis et al., 2012). However, we are aware that although the sample set used here covers the entire hydrothermal fluid evolution path at Qulong (Li et al., 2017b), it is impossible to argue that all stages of mineralization phases have been sampled. In addition,

even though this study arguably presents the most detailed Re-Os geochronology study for a single porphyry Cu-Mo deposit so far, it is very likely that it is still under-sampled. Summarizing, we propose that according to the current study it is likely that the metals at Qulong system were deposited via a cyclic process, but uncertainties remain.

5.4 Rapid cooling during mineralization

Although the A, B and D veins in porphyry copper deposits record the evolution paths of ore-forming fluids (Cooke et al., 2014; Sillitoe, 2010), in most cases the relative chronology of vein types cannot be confidently correlated at the deposit-scale due to a lack of deposit-wide crosscutting relationships. Here, we explore the possibility of coupling high-precision molybdenite Re-Os and quartz fluid inclusion data to reconstruct the cooling paths of the Qulong porphyry system.

Correlating the Re-Os dates in this study and fluid inclusion data (Li et al., 2017b) suggests that the entire hydrothermal system cooled from 425 to 280 °C within 266 ± 13 kyr ($r^2 = 0.797$; Fig. 9). This suggests that the Qulong porphyry system as a whole cooled over the period of ore formation with a cooling rate of 0.55 ± 0.11 °C/kyr. In addition to the long-term cooling trend, the cooling rates of the two complete A-B-D cycles are 1.19 ± 0.82 and 1.27 ± 0.53 °C/kyr, respectively (Fig. 9). A potential concern is an underestimation of the duration caused by the undersampling of Re-Os dates as discussed above, by which the cooling rates could be overestimated. However, we argue that if undersampling is indeed an issue, it is unlikely that the duration will significantly increase given the number and nature (vein type, characteristics of ore related fluid inclusions) of sample set we studied, and the agreement of durations constrained in this study and other independent estimates (see above for detailed discussion). As such we suggest that the estimated cooling rates here, within uncertainties, are reasonable for Qulong. The cooling overrate estimated here propose a

much faster rate than that (0.2 °C/kyr) established from thermochronology (Zhao et al., 2016). Despite the cooling trend of the first mineralization cycle overlaps with that of the long-term cooling rate within uncertainties, the cooling rates of both cycles are much faster than the long-term cooling rate of the Qulong porphyry system. To the best of our knowledge, the cooling rates presented in this study (between 0.55 and 1.27 °C/kyr) are faster than the majority (with the exception of Grasberg) of the reported cooling rates (McInnes et al., 2005; McInnes and Evans, 2005) with highest temporal resolution (<1 % level).

The cooling process of a hydrothermal system is balanced between heat gain (e.g., magmatism injection and volatile fluxing associated with heat from depth) and heat loss (e.g., conduction to wall rocks, cooling by the circulation of meteoric water) (Cathles et al., 1997; Weis et al., 2012). At Qulong, the known thermal contributors are the Rongmucuola pluton, aplite, P porphyry, X porphyry, quartz diorite and exsolved volatile, with heat loss controlled by cooling via conduction. The Rongmucuola pluton, which hosts the majority of the ore at Qulong, is ~1 Myr older than the P porphyry (Fig. 5). Heat loss modelling predicts that a 40 km wide, 2 km thick sill intruded between 16 to 18 km depth can only sustain a maximum hydrothermal discharge >200 °C for 0.8 Myr, and this duration decreases to 1 kyr for systems at shallower depths (<3 - 5 km) (Cathles et al., 1997). Given the much smaller size (<200 m in diameter vs 40 km wide and 2 km thick) and much shallower (potentially ~3 km as inferred from a fluid inclusion study by Li et al., 2017b vs 16 to 18 km) emplacement depth of the Rongmucuola pluton, we conclude that the Rongmucuola pluton was cooled to <200 °C before the emplacement of the P porphyry. As the volumes of the aplite and X porphyry are small, they would have had limited thermal contribution during ore formation as an intrusion with similar size can only sustain a thermal anomaly for less than a few kyr as indicated by quartz titanium diffusion and heat loss models (Cathles et al., 1997; Mercer et al., 2015). As a result, the only possible main thermal contributors are the P porphyry and

exsolved volatile, although we cannot confidently exclude possible contributions from unexposed and unidentified intrusions. With the assumption that the crystallization/cooling process of the P porphyry lasted for less than tens of kyr according to thermal simulation and diffusion modeling (Cathles et al., 1997; Mercer et al., 2015), the $\sim 266 \pm 13$ kyr long thermal anomaly accompanying the mineralization process needs heat sources external to the contribution from the P porphyry itself. Therefore, we suggest that a periodic magmatic-hydrothermal fertilization process, e.g., an episodic hydrothermal fluid release during the incremental building of the source pluton where the metals and magmatic fluids were derived, provided the additional thermal contribution that maintained the mineralization process.

The thermal anomalies and faster cooling process discussed above require a mechanism to explain the rapid heat removal. However, an increase of heat loss through conduction is unlikely, and we suggest that the most reasonable scenario is rapid thermal removal via the meteoric water circulation model (Fekete et al., 2016; Weis et al., 2012). Significant meteoric water circulation is only expected in highly permeable rocks, granitoid units which dominate porphyry deposits are less favorable for such a scenario unless they are intensely fractured. A simple calculation suggests that 10 - 25 volume % meteoric water (~ 100 °C after heating) mixing with 90 - 75 volume % magmatic water is enough to cool the hot (> 500 °C) magmatic fluid to the temperatures recorded by ore-related fluid inclusions (425 - 280 °C). If this is the case, depleted oxygen isotopic composition is expected for the ore-forming fluid at Qulong, which has been demonstrated by our unpublished data and it is the object of a future publication.

Given each mineralization cycle will bring additional heat to the cooling porphyry system, the rapid and periodic cooling process discussed above predicts resetting of thermal chronometers of earlier mineralization cycles by later mineralization cycles. This prediction is supported by the identical Ar-Ar ages of the earlier potassic stage biotite and later phyllic

stage sericite, and the significant scatter of zircon U-Th-He systematics (Zhao et al., 2016), although the uncertainties of these dates do not permit a robust evaluation for the timeframe of these events (e.g., timeframe of formation and cooling history).

5.5 Formation of the world class Qulong Cu-Mo deposit

The detailed high-precision zircon U-Pb and molybdenite Re-Os geochronology presented here allow us to propose a model for the formation of the world-class Qulong porphyry Cu-Mo deposit (Fig. 10).

At ~17 Ma, magma generated in the lower crust was emplaced into the upper crust (the emplacement of the Rongmucuola pluton and the aplite), and was potentially associated with minor mineralization (Fig. 10A). Due to a lack of porphyry stock at this time, the potential conduit transporting magma and volatile to shallow mineralization level is the north-south trending fault. The meteoric water could circulate downward into the system through the fault system.

After the emplacement of the Rongmucuola pluton and aplite, a temporary cessation of magmatism is observed at shallow levels. At ~16 Ma, potentially triggered by a magma injection event, the magma and metal-bearing fluid rose to the shallow crustal levels periodically, as indicated by the formation of mineralization, and the P and X porphyries (Fig. 10B). The formation of these intermineral porphyry stocks may have remobilized/destroyed the earlier mineralization, and resulted in a relatively low Mo grade core within the P porphyry. Episodic volatile releasing events are potentially the trigger of the mechanical failure of the cupola and the upper crust, as evidenced by the formation of two stages of breccia (Fig. 10C). Hydrothermal fluids associated with the breccia pipe caused further alteration and mineralization assemblages, and may have also remobilized/destroyed a portion of earlier stage mineralization. The system is thermally balanced by heat input from

the magmatism and volatiles release events, and heat remove by conduction to wall rock and meteoric water circulation and mixing.

After ~15.860 Ma, the system experienced a further quiet period until ~15.2 Ma. Most likely initiated by injection of new magma that caused thermal rejuvenation, the quartz diorite was formed, which marks the cessation of Miocene magmatism and mineralization at Qulong (Fig. 10D). Minor amount of magmatic fluid associated with the emplacement of the quartz diorite, plus the circulation of meteoric water caused further alteration as represented by the low temperature alteration in the quartz diorite.

6 Implications for porphyry copper system genesis

Radio-isotopic dating is widely applied to constrain the timescales of porphyry copper deposits formation, and give variable timescales from tens of kyr to several Myr (Chiaradia et al., 2014). Given the timescale is a primary feature of the systems studied, which should be an independent parameter regardless of the dating methods used, the strong positive relationship between analytical precision and the quoted duration is not expected (Fig. 11). Therefore, this relationship (Fig. 11) suggests that at least some of the prolonged durations proposed for porphyry systems may be an artefact of over interpreting low-precision data without evaluation of their accuracy. Recent simulation studies suggest that the duration of ore formation is potentially one the of controlling factors for the formation of giant deposits (Chelle-Michou et al., 2017; Chiaradia and Caricchi, 2017). However, it is obvious that such a “long” duration (e.g., tens to hundreds of kyr) is still beyond the precision of micro-beam analysis (Chiaradia et al., 2014). Consequently, we reiterate that high-precision geochronology is essential for resolving the magmatic-mineralization timescales of porphyry copper systems at the tens of kyr level.

808 The genetic model of porphyry copper deposits suggests that the porphyry stocks are
809 the conduits conveying metal-bearing volatile from the lower crustal magma chamber to
810 shallow levels (Cooke et al., 2014; Richards, 2011; Sillitoe, 2010). However, in most cases
811 this scenario is very difficult to test by crosscutting relationship for two reasons. First, the
812 porphyry stock is exceptionally small compared to the size of the deposit (Cooke et al., 2014;
813 Richards, 2011; Sillitoe, 2010), such that the crosscutting relationship between the porphyry
814 stock and mineralization phases are only available in a very limited space, e.g., surrounding
815 the porphyry stock. Secondly, if there are mineralization phases before the emplacement of
816 the porphyry stock, they will likely be overprinted/remobilized/destroyed by the
817 emplacement of the porphyry stock where the potential crosscutting relationships are
818 available. Therefore, the best approach to test this hypothesis is via high precision dating, and
819 our high precision dating at Qulong arguably suggests that it is possible to transport metal-
820 bearing volatile without the presence of a contemporary porphyry stock. This scenario has
821 been supported by observations at modern volcanoes whereby degassing can occur
822 before/without magma eruption at shallow levels (Shinohara, 2008). If this finding is correct,
823 it further suggests that the absence of a contemporary porphyry stock does not indicate that
824 the mineralization is not a porphyry style deposit, which has broad implication for deposit
825 type clarification and mineral exploration. In addition, the presence of mineralization before
826 the emplacement of a porphyry stock or even the absence of porphyry stocks implies that
827 dating porphyry stocks does not necessarily brackets the entire porphyry ore formation
828 process. In this case dating the mineralization directly is critical to yield a comprehensive
829 understanding of the timescale of ore formation, as well as of any associated magmatism
830 (Stein, 2014).

831 The cyclic mineralization process inferred by our Re-Os dates suggests that the
832 periodic mineralization process also operates for deposits with a short duration (e.g.,

hundreds of kyr overall duration), which is the same as those observed in porphyry systems with prolonged (Myr level) duration (Spencer et al., 2015; Stein, 2014; Zimmerman et al., 2014). Cyclic magmatic process in porphyry Cu deposits is ubiquitously recorded in many magmatic minerals, e.g., zoning/resorption textures of plagioclase, quartz and zircon (Buret et al., 2016; Mercer et al., 2015; Tapster et al., 2016; Williamson et al., 2016). By inference, we suggest that the periodic magmatic-hydrothermal processes during ore formation proposed here are common in porphyry copper deposits, and are linked with the episodic magmatic process occurring at depth within the source pluton. The significance of this cyclic process is that each mineralization pulse can enhance the economic resource in a geologically focused area. As such, the cyclic process presented here potentially is one of the contributing factors to form giant deposits, and is the key to differentiate economic and sub-economic deposits. However, it is not clear yet what fundamentally controls this cyclic process, although the periodic re-fertilization of volatile linked with source pluton evolution might be critical (Williamson et al., 2016).

The cyclic cooling process proposed here, together with the potential thermal resetting of the U-Th-He and Ar-Ar chronometers, should be considered in future cooling history studies of porphyry copper systems. In addition, the rapid cooling (0.55 - 1.27 °C/kyr) and periodic volatile recharge process proposed here suggest that external fluid potentially is a critical cooling agent, as recently proposed by numerical modeling and isotopic study of porphyry deposits (Fekete et al., 2016; Weis et al., 2012).

A final note concerns the uncertainties when comparing Re-Os dates from different labs and with U-Pb and other chronometers. Reporting the measured values of the RM8599 is a must to evaluate the (relative) accuracy of the Re-Os dates (Stein, 2014), and also the analysis of a suitable sized aliquant from a mineral separate is of primary importance (Selby and Creaser, 2004; Stein et al., 2003). Currently the decay constant uncertainties (^{238}U and

¹⁸⁷Re) are the main source of uncertainties when comparing Re-Os and U-Pb systems. In addition, the inter-laboratory agreement of Re-Os systems has only been demonstrated between a few labs (Markey et al., 2007), so direct comparison of dates beyond these laboratories potentially involves an unaccounted bias. Given that significant progress has been achieved for the precision and accuracy of the zircon U-Pb chronometers in the past ten years via the community-driven EARTHTIME initiative (Condon et al., 2015; McLean et al., 2015), and the analytical precision of molybdenite Re-Os system is down to 1 ‰, now it is an appropriate time to start a further evaluation between the molybdenite Re-Os and zircon U-Pb systems (Selby et al., 2007) as suggested by Chiaradia et al. (2014). Following the example of the U-Pb community, shared tracer/reference solutions and transparent data reduction platform should be adopted in the Re-Os community with the aim to standardize the Re-Os chronometer, reduce the potential bias between laboratories and ultimately improve the accuracy. Once achieved, data from all laboratories can be integrated without loss of resolution (due to inter-laboratory bias) and will enable better utilization of data from the literature.

Acknowledgements

YL thanks Prof. Xian-Hua Li for his continuing supporting, encouragement and supervision. YL acknowledges Richard Sillitoe and Jeremy Richards for generously sharing their expertise in ore-forming process and guidance regarding the clarification of veinlets. Access to Qulong is only possible with assistance from You-Ye Zheng, Guang-Wu Jiang, Jian-Wei Li, Zhi-Ming Yang and Ke-Zhang Qin. Rui Wang and Jia Chang are acknowledged for support in the field. YL was financially funded by DU and CSC, with grant-in-aid from SEG, IAGC, GSL, UCCL and University College of Durham. A NERC facility grant awarded to DS and YL funded the U-Pb study. DS acknowledges the Total Endowment Fund.

1
2
3
4
5
6
7
8
9
10
11
12
13
14
15
16
17
18
19
20
21
22
23
24
25
26
27
28
29
30
31
32
33
34
35
36
37
38
39
40
41
42
43
44
45
46
47
48
49
50
51
52
53
54
55
56
57
58
59
60
61
62
63
64
65

883 An early version of the paper benefits from the comments from Derek Vance and an
884 anonymous reviewer. Constructive suggestions from Cyril Chelle-Michou and an anonymous
885 reviewer, plus comments from editors Massimo Chiaradia and Larry Meinert greatly
886 improved the quality of this final version and are appreciated.

References

- Birck, J.L., RoyBarman, M., Capmas, F., 1997. Re-Os isotopic measurements at the femtomole level in natural samples. *Geostandard Newslett* 21, 19-27.
- Bowring, J., McLean, N.M., Bowring, S., 2011. Engineering cyber infrastructure for U - Pb geochronology: Tripoli and U - Pb_Redux. *Geochemistry, Geophysics, Geosystems* 12.
- Buret, Y., von Quadt, A., Heinrich, C., Selby, D., Walle, M., Peytcheva, I., 2016. From a long-lived upper-crustal magma chamber to rapid porphyry copper-emplacement: Reading the geochemistry of zircon crystals at Bajo de la Alumbrera (NW Argentina). *Earth and Planetary Science Letters* 450, 120-131.
- Burnham, A.D., Berry, A.J., 2012. An experimental study of trace element partitioning between zircon and melt as a function of oxygen fugacity. *Geochimica Et Cosmochimica Acta* 95, 196-212.
- Cathles, L.M., 1977. An analysis of the cooling of intrusives by ground-water convection which includes boiling. *Economic Geology* 72, 804-826.
- Cathles, L.M., Erendi, A.H.J., Barrie, T., 1997. How long can a hydrothermal system be sustained by a single intrusive event? *Economic Geology* 92, 766-771.
- Chelle-Michou, C., Chiaradia, M., Ovtcharova, M., Ulianov, A., Wotzlaw, J.F., 2014. Zircon petrochronology reveals the temporal link between porphyry systems and the magmatic evolution of their hidden plutonic roots (the Eocene Corocochuayco deposit, Peru). *Lithos* 198, 129-140.
- Chelle-Michou, C., Chiaradia, M., Selby, D., Ovtcharova, M., Spikings, R.A., 2015. High-Resolution Geochronology of the Corocochuayco Porphyry-Skarn Deposit, Peru: A Rapid Product of the Incaic Orogeny. *Economic Geology* 110, 423-443.
- Chelle-Michou, C., Rottier, B., Caricchi, L., Simpson, G., 2017. Tempo of magma degassing and the genesis of porphyry copper deposits. *Sci Rep* 7, 40566.
- Cheng, H., Edwards, R.L., Hoff, J., Gallup, C.D., Richards, D.A., Asmerom, Y., 2000. The half-lives of uranium-234 and thorium-230. *Chemical Geology* 169, 17-33.
- Chiaradia, M., Caricchi, L., 2017. Stochastic modelling of deep magmatic controls on porphyry copper deposit endowment. *Scientific Reports* 7, 44523.
- Chiaradia, M., Schaltegger, U., Spikings, R., 2014. Time Scales of Mineral Systems-Advances in Understanding Over the Past Decade. *Soc Econ Geol Spec P*, 37-58.
- Cohen, A.S., Waters, F.G., 1996. Separation of osmium from geological materials by solvent extraction for analysis by thermal ionisation mass spectrometry. *Analytica Chimica Acta* 332, 269-275.
- Condon, D.J., Schoene, B., McLean, N.M., Bowring, S.A., Parrish, R.R., 2015. Metrology and traceability of U-Pb isotope dilution geochronology (EARTHTIME Tracer Calibration Part I). *Geochimica Et Cosmochimica Acta* 164, 464-480.

- Cooke, D.R., Hollings, P., Wilkinson, J.J., Tosdal, R.M., 2014. 13.14 - Geochemistry of Porphyry Deposits, in: Turekian, H.D.H.K. (Ed.), *Treatise on Geochemistry* (Second Edition). Elsevier, Oxford, pp. 357-381.
- Creaser, R.A., Papanastassiou, D.A., Wasserburg, G.J., 1991. Negative Thermal Ion Mass-Spectrometry of Osmium, Rhenium, and Iridium. *Geochimica Et Cosmochimica Acta* 55, 397-401.
- Cumming, V.M., Poulton, S.W., Rooney, A.D., Selby, D., 2013. Anoxia in the terrestrial environment during the late Mesoproterozoic. *Geology* 41, 583-586.
- Deckart, K., Clark, A.H., Cuadra, P., Fanning, M., 2012. Refinement of the time-space evolution of the giant Mio-Pliocene Río Blanco-Los Bronces porphyry Cu–Mo cluster, Central Chile: new U–Pb (SHRIMP II) and Re–Os geochronology and $^{40}\text{Ar}/^{39}\text{Ar}$ thermochronology data. *Mineralium Deposita* 48, 57-79.
- Fekete, S., Weis, P., Driesner, T., Bouvier, A.S., Baumgartner, L., Heinrich, C.A., 2016. Contrasting hydrological processes of meteoric water incursion during magmatic-hydrothermal ore deposition: An oxygen isotope study by ion microprobe. *Earth and Planetary Science Letters* 451, 263-271.
- Gerstenberger, H., Haase, G., 1997. A highly effective emitter substance for mass spectrometric Pb isotope ratio determinations. *Chemical Geology* 136, 309-312.
- Gustafson, L.B., Hunt, J.P., 1975. The porphyry copper deposit at El Salvador, Chile. *Economic Geology* 70, 857-912.
- Hiess, J., Condon, D.J., McLean, N., Noble, S.R., 2012. $^{238}\text{U}/^{235}\text{U}$ Systematics in terrestrial uranium-bearing minerals. *Science* 335, 1610-1614.
- Hou, Z.Q., Gao, Y.F., Qu, X.M., Rui, Z.Y., Mo, X.X., 2004. Origin of adakitic intrusives generated during mid-Miocene east-west extension in southern Tibet. *Earth and Planetary Science Letters* 220, 139-155.
- Hou, Z.Q., Yang, Z.M., Qu, X.M., Meng, X.J., Li, Z.Q., Beaudoin, G., Rui, Z.Y., Gao, Y.F., Zaw, K., 2009. The Miocene Gangdese porphyry copper belt generated during post-collisional extension in the Tibetan Orogen. *Ore Geology Reviews* 36, 25-51.
- Hu, Y.B., Liu, J.Q., Ling, M.X., Ding, W., Liu, Y., Zartman, R.E., Ma, X.F., Liu, D.Y., Zhang, C.C., Sun, S.J., Zhang, L.P., Wu, K., Sun, W.D., 2015. The formation of Qulong adakites and their relationship with porphyry copper deposit: Geochemical constraints. *Lithos* 220, 60-80.
- Jaffey, A.H., Flynn, K.F., Glendenin, L.E., Bentley, W.C., Essling, A.M., 1971. Precision Measurement of Half-Lives and Specific Activities of ^{235}U and ^{238}U . *Physical Review C* 4, 1889-1906.
- Klötzli, U., Klötzli, E., Günes, Z., Kosler, J., 2009. Accuracy of Laser Ablation U–Pb Zircon Dating: Results from a Test Using Five Different Reference Zircons. *Geostandards and Geoanalytical Research* 33, 5-15.

- Krogh, T., 1973. A low-contamination method for hydrothermal decomposition of zircon and extraction of U and Pb for isotopic age determinations. *Geochimica et cosmochimica acta* 37, 485-494.
- Lawley, C.J.M., Selby, D., 2012. Re-Os geochronology of quartz-enclosed ultrafine molybdenite: implications for ore geochronology. *Economic Geology* 107, 1499-1505.
- Li, X.H., Liu, X.M., Liu, Y.S., Su, L., Sun, W.D., Huang, H.Q., Yi, K., 2015. Accuracy of LA-ICPMS zircon U-Pb age determination: An inter-laboratory comparison. *Sci China Earth Sci* 58, 1722-1730.
- Li, Y., Li, J.W., Li, X.H., Selby, D., Huang, G.H., Chen, L.J., Zheng, K., 2017a. An Early Cretaceous carbonate replacement origin for the Xinqiao stratabound massive sulfide deposit, Middle-Lower Yangtze Metallogenic Belt, China. *Ore Geology Reviews* 80, 985-1003.
- Li, Y., Selby, D., Feely, M., Costanzo, A., Li, X.-H., 2017b. Fluid inclusion characteristics and molybdenite Re-Os geochronology of the Qulong porphyry copper-molybdenum deposit, Tibet. *Mineralium Deposita* 52, 137-158.
- Luo, Y., Ayers, J.C., 2009. Experimental measurements of zircon/melt trace-element partition coefficients. *Geochimica Et Cosmochimica Acta* 73, 3656-3679.
- Markey, R., Stein, H.J., Hannah, J.L., Zimmerman, A., Selby, D., Creaser, R.A., 2007. Standardizing re-os geochronology: A new molybdenite reference material (Henderson, USA) and the stoichiometry of Os salts. *Chemical Geology* 244, 74-87.
- Matthews, A., Riley, J., 1970. The determination of rhenium in sea water. *Analytica Chimica Acta* 51, 483-488.
- Mattinson, J.M., 2005. Zircon U-Pb chemical abrasion ("CA-TIMS") method: Combined annealing and multi-step partial dissolution analysis for improved precision and accuracy of zircon ages. *Chemical Geology* 220, 47-66.
- McInnes, B.I., Evans, N.J., Fu, F., Garwin, S., Belousova, E., Griffin, W., Bertens, A., Sukarna, D., Permanadewi, S., Andrew, R., 2005. Thermal history analysis of selected Chilean, Indonesian, and Iranian porphyry Cu-Mo-Au deposits. *Super Porphyry Copper and Gold Deposits: A Global Perspective* (Porter, TM; editor). Porter Geoconsultancy Publishing, de Adelaide, Australia, 27-42.
- McInnes, B.I.A., Evans, N.J., 2005. Application of thermochronology to hydrothermal ore deposits. *Low-Temperature Thermochronology: Techniques, Interpretations, and Applications* 58, 467-498.
- McLean, N.M., Bowring, J.F., Bowring, S.A., 2011. An algorithm for U-Pb isotope dilution data reduction and uncertainty propagation. *Geochemistry Geophysics Geosystems* 12, n/a-n/a.
- McLean, N.M., Condon, D.J., Schoene, B., Bowring, S.A., 2015. Evaluating uncertainties in the calibration of isotopic reference materials and multi-element isotopic tracers (EARTHTIME Tracer Calibration Part II). *Geochimica Et Cosmochimica Acta* 164, 481-501.

- 1000 Mercer, C.N., Reed, M.H., Mercer, C.M., 2015. Time Scales of Porphyry Cu Deposit
11001 Formation: Insights from Titanium Diffusion in Quartz. *Economic Geology* 110, 587-602.
2
- 31002 Morgan, J.W., Golightly, D.W., Dorrzapf, A.F., 1991. Methods for the Separation of
41003 Rhenium, Osmium and Molybdenum Applicable to Isotope Geochemistry. *Talanta* 38, 259-
51004 265.
61004
7
- 81005 Nier, A.O., 1950. A redetermination of the relative abundances of the isotopes of carbon,
91006 nitrogen, oxygen, argon, and potassium. *Physical Review* 77, 789.
10
- 111007 Richards, J.P., 2011. Magmatic to hydrothermal metal fluxes in convergent and collided
121008 margins. *Ore Geology Reviews* 40, 1-26.
131008
14
- 151009 Richards, J.P., 2015. Tectonic, magmatic, and metallogenic evolution of the Tethyan orogen:
161010 From subduction to collision. *Ore Geology Reviews* 70, 323-345.
17
- 181011 Roy-Barman, M., 1993. Mesure du rapport $^{187}\text{Os}/^{186}\text{Os}$ dans les basaltes et les péridotites:
191012 contribution à la systématique $^{187}\text{Re}/^{187}\text{Os}$ dans le manteau. Paris 7.
201012
21
- 221013 Rubatto, D., Hermann, J., 2007. Experimental zircon/melt and zircon/garnet trace element
231014 partitioning and implications for the geochronology of crustal rocks. *Chemical Geology* 241,
241015 38-61.
251015
26
- 271016 Schaltegger, U., Schmitt, A.K., Horstwood, M.S.A., 2015. U-Th-Pb zircon geochronology by
281017 ID-TIMS, SIMS, and laser ablation ICP-MS: Recipes, interpretations, and opportunities.
291018 *Chemical Geology* 402, 89-110.
30
- 311019 Schärer, U., 1984. The effect of initial ^{230}Th disequilibrium on young UPb ages: the Makalu
321020 case, Himalaya. *Earth and Planetary Science Letters* 67, 191-204.
331020
34
- 351021 Schoene, B., 2014. 4.10 - U-Th-Pb Geochronology, in: Turekian, H.D.H.K. (Ed.), *Treatise*
361022 *on Geochemistry* (Second Edition). Elsevier, Oxford, pp. 341-378.
37
- 381023 Selby, D., Creaser, R.A., 2001. Re-Os geochronology and systematics in molybdenite from
391024 the Endako porphyry molybdenum deposit, British Columbia, Canada. *Economic Geology*
401024 and the *Bulletin of the Society of Economic Geologists* 96, 197-204.
411025
42
- 431026 Selby, D., Creaser, R.A., Stein, H.J., Markey, R.J., Hannah, J.L., 2007. Assessment of the
441027 ^{187}Re decay constant by cross calibration of Re-Os molybdenite and U-Pb zircon
451028 chronometers in magmatic ore systems. *Geochimica et Cosmochimica Acta* 71, 1999-2013.
461028
47
- 481029 Shen, J.J., Papanastassiou, D.A., Wasserburg, G.J., 1996. Precise Re-Os determinations and
491030 systematics of iron meteorites. *Geochimica Et Cosmochimica Acta* 60, 2887-2900.
50
- 511031 Shinohara, H., 2008. Excess Degassing from Volcanoes and Its Role on Eruptive and
521032 Intrusive Activity. *Reviews of Geophysics* 46, n/a-n/a.
531032
54
- 551033 Shirey, S.B., Walker, R.J., 1995. Carius Tube Digestion for Low-Blank Rhenium-Osmium
561034 Analysis. *Analytical Chemistry* 67, 2136-2141.
57
- 581035 Sillitoe, R.H., 2000. Gold-rich porphyry deposits: descriptive and genetic models and their
591036 role in exploration and discovery. *Reviews in Economic Geology* 13, 315-345.
601036
61
62
63
64
65

- Sillitoe, R.H., 2010. Porphyry Copper Systems. *Economic Geology* 105, 3-41.
- Sillitoe, R.H., Mortensen, J.K., 2010. Longevity of Porphyry Copper Formation at Quellaveco, Peru. *Economic Geology* 105, 1157-1162.
- Smoliar, M.I., Walker, R.J., Morgan, J.W., 1996. Re-Os ages of group IIA, IIIA, IVA, and IVB iron meteorites. *Science* 271, 1099-1102.
- Spencer, E.T., Wilkinson, J.J., Creaser, R.A., Seguel, J., 2015. The Distribution and Timing of Molybdenite Mineralization at the El Teniente Cu-Mo Porphyry Deposit, Chile. *Economic Geology* 110, 387-421.
- Stein, H.J., 2006. Low-rhenium molybdenite by metamorphism in northern Sweden: Recognition, genesis, and global implications. *Lithos* 87, 300-327.
- Stein, H.J., 2014. 13.4 - Dating and Tracing the History of Ore Formation, in: Turekian, H.D.H.K. (Ed.), *Treatise on Geochemistry (Second Edition)*. Elsevier, Oxford, pp. 87-118.
- Stein, H.J., Markey, R.J., Morgan, J.W., Hannah, J.L., Schersten, A., 2001. The remarkable Re-Os chronometer in molybdenite: how and why it works. *Terra Nova* 13, 479-486.
- Tapster, S., Condon, D.J., Naden, J., Noble, S.R., Petterson, M.G., Roberts, N.M.W., Saunders, A.D., Smith, D.J., 2016. Rapid thermal rejuvenation of high-crystallinity magma linked to porphyry copper deposit formation; evidence from the Koloula Porphyry Prospect, Solomon Islands. *Earth and Planetary Science Letters* 442, 206-217.
- Völkening, J., Walczyk, T., Heumann, K.G., 1991. Osmium isotope ratio determinations by negative thermal ionization mass spectrometry. *International Journal of Mass Spectrometry and Ion Processes* 105, 147-159.
- von Quadt, A., Erni, M., Martinek, K., Moll, M., Peytcheva, I., Heinrich, C.A., 2011. Zircon crystallization and the lifetimes of ore-forming magmatic-hydrothermal systems. *Geology* 39, 731-734.
- Wang, L.-L., Mo, X.-X., B, L., G-C, D., Zhao, Z.-D., 2006. Geochronology and geochemistry of the ore-bearing porphyry in Qulong Cu (Mo) deposit, Tibet. *Acta Petrologica Sinica* 22, 1001-1008.
- Wang, R., Richards, J.P., Hou, Z.Q., Yang, Z.M., 2014. Extent of underthrusting of the Indian plate beneath Tibet controlled the distribution of Miocene porphyry Cu-Mo +/- Au deposits. *Mineralium Deposita* 49, 165-173.
- Wang, R., Richards, J.P., Zhou, L.M., Hou, Z.Q., Stern, R.A., Creaser, R.A., Zhu, J.J., 2015. The role of Indian and Tibetan lithosphere in spatial distribution of Cenozoic magmatism and porphyry Cu-Mo deposits in the Gangdese belt, southern Tibet. *Earth-Science Reviews* 150, 68-94.
- Weis, P., 2015. The dynamic interplay between saline fluid flow and rock permeability in magmatic-hydrothermal systems. *Geofluids* 15, 350-371.
- Weis, P., Driesner, T., Heinrich, C.A., 2012. Porphyry-copper ore shells form at stable pressure-temperature fronts within dynamic fluid plumes. *Science* 338, 1613-1616.

- Wendt, I., Carl, C., 1991. The Statistical Distribution of the Mean Squared Weighted Deviation. *Chemical Geology* 86, 275-285.
- Williamson, B.J., Herrington, R.J., Morris, A., 2016. Porphyry copper enrichment linked to excess aluminium in plagioclase. *Nature Geoscience* 9, 237-U169.
- Xiao, B., Qin, K.Z., Li, G.M., Li, J.X., Xia, D.X., Chen, L., Zhao, J.X., 2012. Highly Oxidized Magma and Fluid Evolution of Miocene Qulong Giant Porphyry Cu-Mo Deposit, Southern Tibet, China. *Resource Geology* 62, 4-18.
- Yang, Z.M., Hou, Z.Q., White, N.C., Chang, Z.S., Li, Z.Q., Song, Y.C., 2009. Geology of the post-collisional porphyry copper-molybdenum deposit at Qulong, Tibet. *Ore Geology Reviews* 36, 133-159.
- Yang, Z.M., Lu, Y.J., Hou, Z.Q., Chang, Z.S., 2015. High-Mg Diorite from Qulong in Southern Tibet: Implications for the Genesis of Adakite-like Intrusions and Associated Porphyry Cu Deposits in Collisional Orogens. *Journal of Petrology* 56, 227-253.
- Yin, Q.Z., Jacobsen, S.B., Lee, C.T., McDonough, W.F., Rudnick, R.L., Horn, I., 2001. A gravimetric K₂OsCl₆ standard: Application to precise and accurate Os spike calibration. *Geochimica Et Cosmochimica Acta* 65, 2113-2127.
- Zhang, Z.M., Dong, X., Santosh, M., Zhao, G.C., 2014. Metamorphism and tectonic evolution of the Lhasa terrane, Central Tibet. *Gondwana Research* 25, 170-189.
- Zhao, J., Qin, K., Xiao, B., McInnes, B., Li, G., Evans, N., Cao, M., Li, J., 2016. Thermal history of the giant Qulong Cu–Mo deposit, Gangdese metallogenic belt, Tibet: Constraints on magmatic–hydrothermal evolution and exhumation. *Gondwana Research* 36, 390-409.
- Zheng, Y.Y., Sun, X., Gao, S.B., Wu, S., Xu, J., Jiang, J.S., Chen, X., Zhao, Z.Y., Liu, Y., 2015. Metallogenesis and the minerogenetic series in the Gangdese polymetallic copper belt. *Journal of Asian Earth Sciences* 103, 23-39.
- Zheng, Y.Y., Xue, Y.X., Cheng, L.J., Fan, Z.H., Gao, S.B., 2004. Finding, Characteristics and Significances of Qulong Superlarge Porphyry Copper (Molybdenum) Deposit, Tibet. *Earth Sciences* 29, 103-108 (In Chinese with English Abstract).
- Zhu, D.C., Wang, Q., Zhao, Z.D., Chung, S.L., Cawood, P.A., Niu, Y., Liu, S.A., Wu, F.Y., Mo, X.X., 2015. Magmatic record of India-Asia collision. *Sci Rep* 5, 14289.
- Zimmerman, A., Stein, H.J., Morgan, J.W., Markey, R.J., Watanabe, Y., 2014. Re–Os geochronology of the El Salvador porphyry Cu–Mo deposit, Chile: Tracking analytical improvements in accuracy and precision over the past decade. *Geochimica et Cosmochimica Acta* 131, 13-32.

List of figures and Tables

Fig. 1. Geological setting of the Lhasa terrane and deposit geology map of Qulong porphyry Cu-Mo deposit. A) Simplified geological setting of the Lhasa terrane, Gangdese Magmatic Belt and Gangdese Porphyry Copper Deposits Belt. B) Geological map of the Qulong porphyry Cu-Mo deposit. C) Cross section showing the crosscutting relationship of the Miocene units at the Qulong porphyry Cu-Mo deposit. D-E) Cross section showing the Cu and Mo grades. Revised after Yang et al. (2009) and Zhao et al. (2016).

Fig. 2. Geological timeframe of the intrusion and mineralization at Qulong constrained by crosscutting relationships and geochronology. A) Relative chronology of the Miocene magmatism and mineralization at Qulong porphyry Cu-Mo deposit. B) Published geochronology data of the Miocene magmatism and mineralization at Qulong porphyry Cu-Mo deposit. See text for discussion. Detailed dates are provided in Table A1 - A2. For source of dates, 1, Hu et al., 2015. 2, Wang et al., 2006. 3, Li et al., 2004. 4, Zhao et al., 2015. 5, Hou et al., 2004. 6, Li et al., 2017. Revised after Li et al. (2017b).

Fig. 3. Petrography of the Rongmucuola pluton (A), the P porphyry (B), and post-ore quartz diorite (C). CL images of the analyzed zircon grains of the Rongmucuola pluton, the P porphyry and the quartz diorite (D).

Fig. 4. Representative A (A), B (B) and D (D) veins from the Qulong porphyry Cu-Mo deposit. A) The A veins are characterized by 0.3 - 0.8 cm wide discontinuous granular quartz veinlets with narrow (< 3 mm) K-feldspar selvages, which host disseminated chalcopyrite and molybdenite; B) The B veins are represented by veinlets (0.4 - 2 cm wide) comprising crystalline quartz with suture in the centre, and possess irregularly distributed K-feldspar selvage, and predominantly host molybdenite and chalcopyrite along the margin of the vein; C) The definition of vein types are illustrated following those of Gustafson and Hunt (1975) and Sillitoe (2010). D) The D quartz veins (0.5 - 6 cm) host euhedral pyrite, with sericite and anhydrite (0.1 and 1.5 cm) selvages, and minor disseminated chalcopyrite and molybdenite. E-F) Representative sections showing the crosscutting relationships between different stages of veins, e.g., A type quartz vein cut by later A and B type veins. See text for details.

Fig. 5. The impact of Th disequilibrium correction as illustrated by the youngest group of zircon dates of the P porphyry. A) the weighted mean of the youngest three dates as a function of variable Th/U values used for Th disequilibrium correction. B) the MSWD of the weighted mean of the youngest three dates as a function of the variable Th/U values used for

Th disequilibrium correction. Also showing in the figures are the applied Th/U value with uncertainty for the P porphyry (see text for detailed discussion).

Fig. 6. A) Cartoon illustrating the approach of obtaining several independent molybdenite separates from a single vein, which permits testing the consistency of Re-Os systematics along the vein, verify the accuracy of the Re-Os ages and reducing analytical uncertainties. B) The multiple independent molybdenite separates approach illustrated by a B vein analysed in this study. C) The model ages of the Henderson molybdenite reference materials (RM8599) analysed during the course of study, which yield a weighted mean age of 27.695 ± 0.038 ($n = 9$, MSWD = 0.53) and overlap with the recommended value of 27.66 ± 0.10 (Markey et al., 2007; Zimmerman et al., 2014).

Fig. 7. The CA-ID-TIMS U-Pb zircon dates of the Rongmucuola pluton, the P porphyry and the quartz diorite at Qulong porphyry Cu-Mo deposit. A) The Wetherill Concordia diagram of the analysed zircon grains. B) $^{206}\text{Pb}/^{238}\text{U}$ ages of the analysed zircon grains and the weighted mean ages of the Rongmucuola pluton, the P porphyry and post-ore quartz diorite.

Fig. 8. The ID-NTIMS molybdenite Re-Os geochronology data of molybdenite veins at Qulong, with probability density plot of different type of veins shown.

Fig. 9. Cooling history of Qulong porphyry Cu-Mo system during ore formation, with vein-formation ages and temperatures constrained by molybdenite Re-Os dating in this study and fluid inclusion data of Li et al. (2017b). The uncertainties of fluid inclusions are shown as ± 10 °C (1 sigma), while the uncertainties of Re-Os dates are smaller than the width of the symbol.

Fig. 10. Cartoon showing the genetic model of the Qulong porphyry Cu-Mo deposit. See figure and text for detailed information.

Fig. 11. Analytical precision used in porphyry copper deposits studies and inferred timescales exhibiting a positive relationship. Data are from Chiaradia et al. (2014). See text for discussion.

Table 1. CA-ID-TIMS U-Pb data of Miocene intrusive rocks at Qulong.

Table 2. Re-Os data of molybdenite samples from Qulong.

1171

1
2 1172 Supplementary tables

3
4 1173 Table A1, Published zircon U-Pb geochronology dates at Qulong

5
6 1174 Table A2, Published molybdenite Re-Os and zircon U-Th-He geochronology dates at Qulong

7

8

9

10

11

12

13

14

15

16

17

18

19

20

21

22

23

24

25

26

27

28

29

30

31

32

33

34

35

36

37

38

39

40

41

42

43

44

45

46

47

48

49

50

51

52

53

54

55

56

57

58

59

60

61

62

63

64

65

Fig. 1

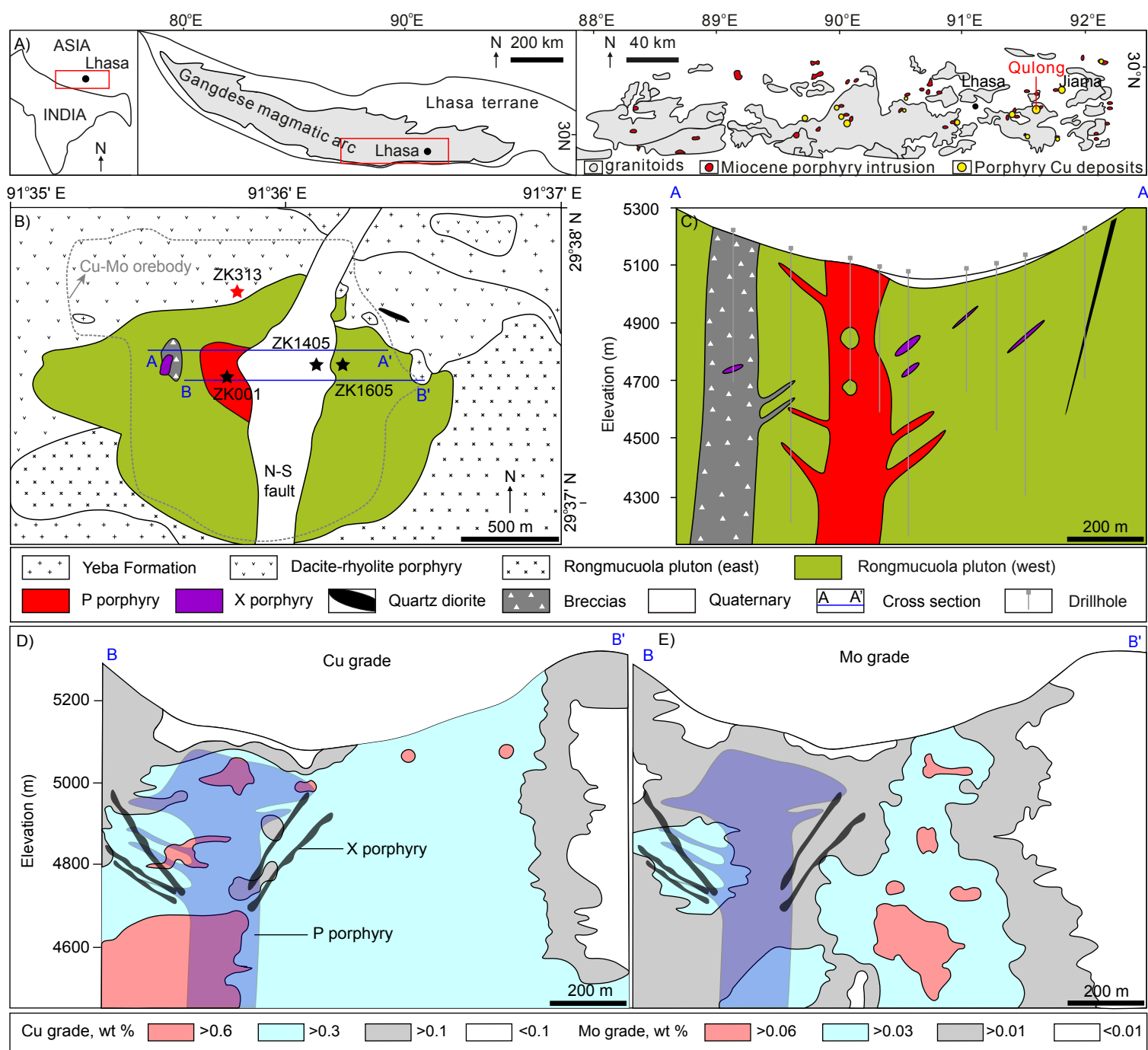


Fig. 2

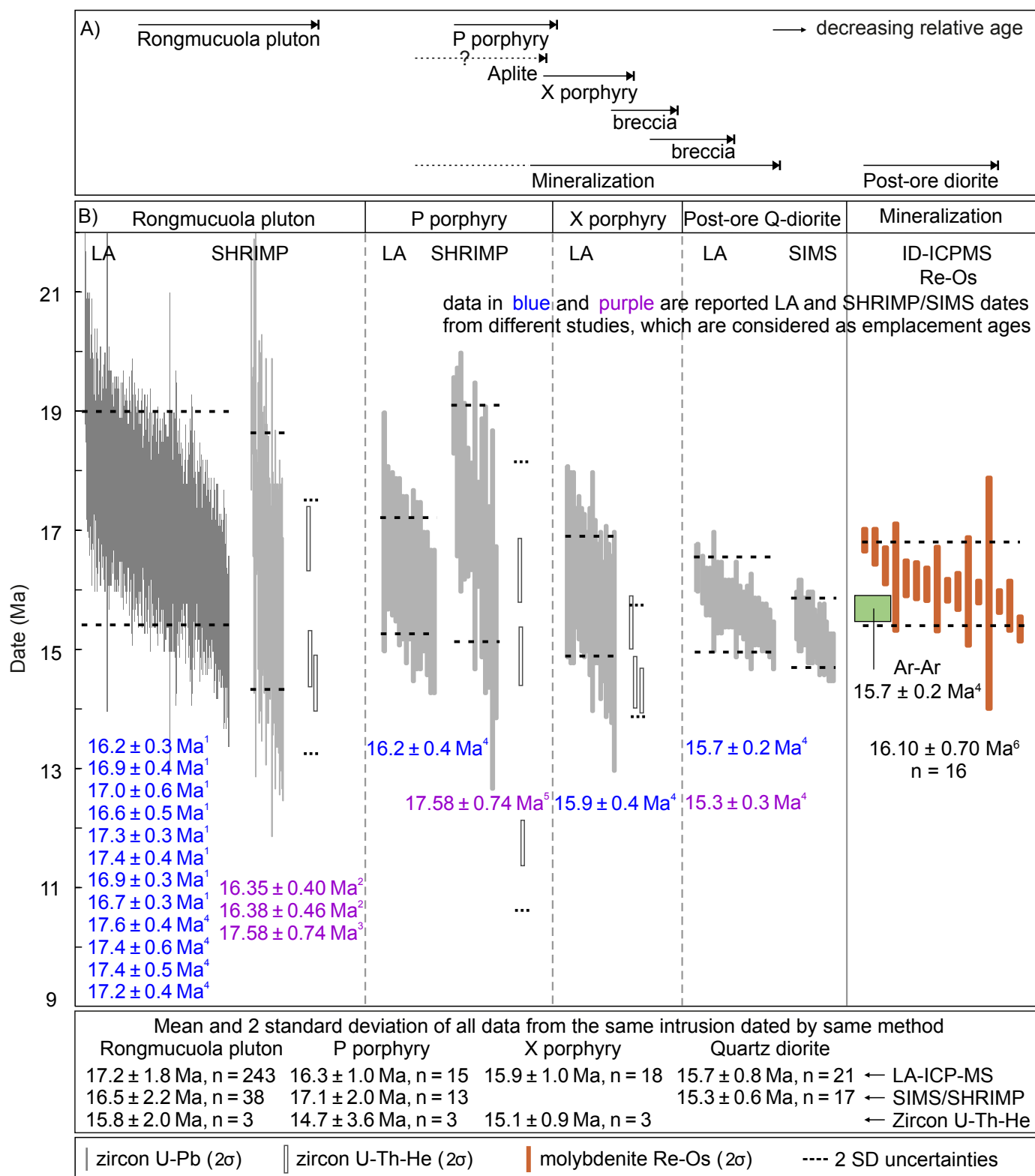


Fig. 3

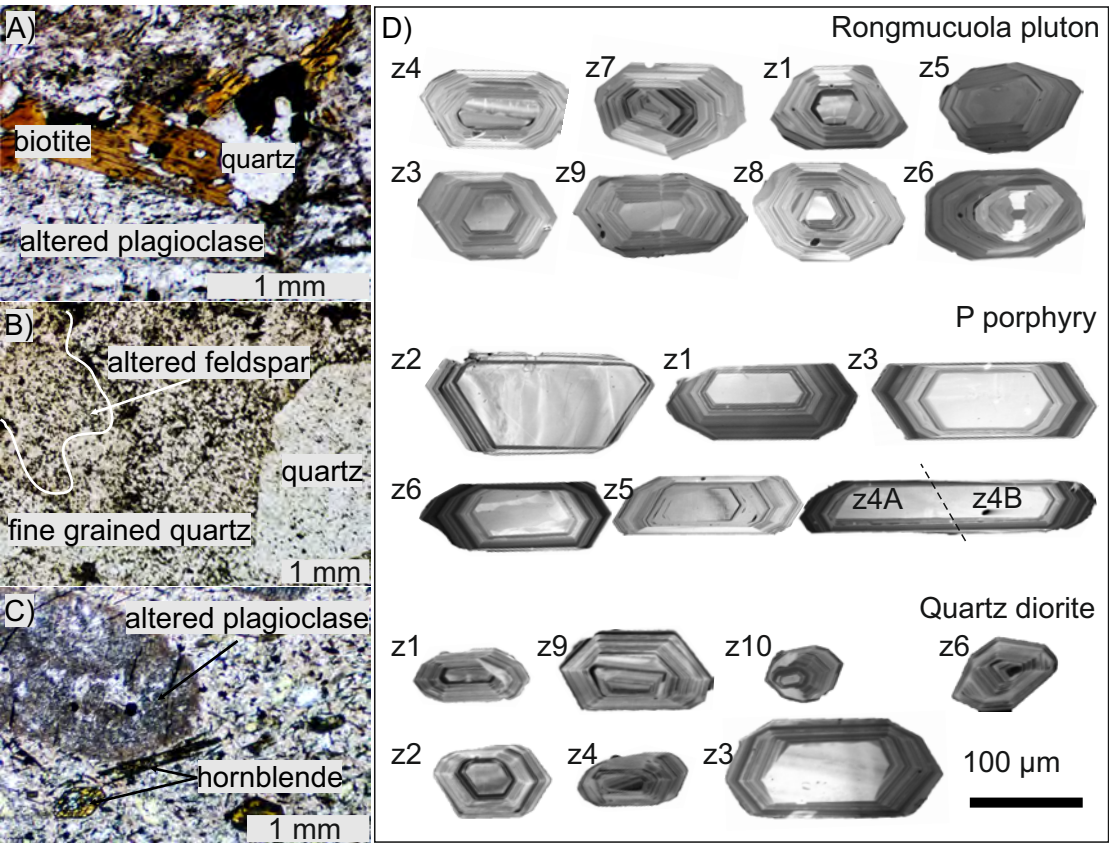


Fig. 4

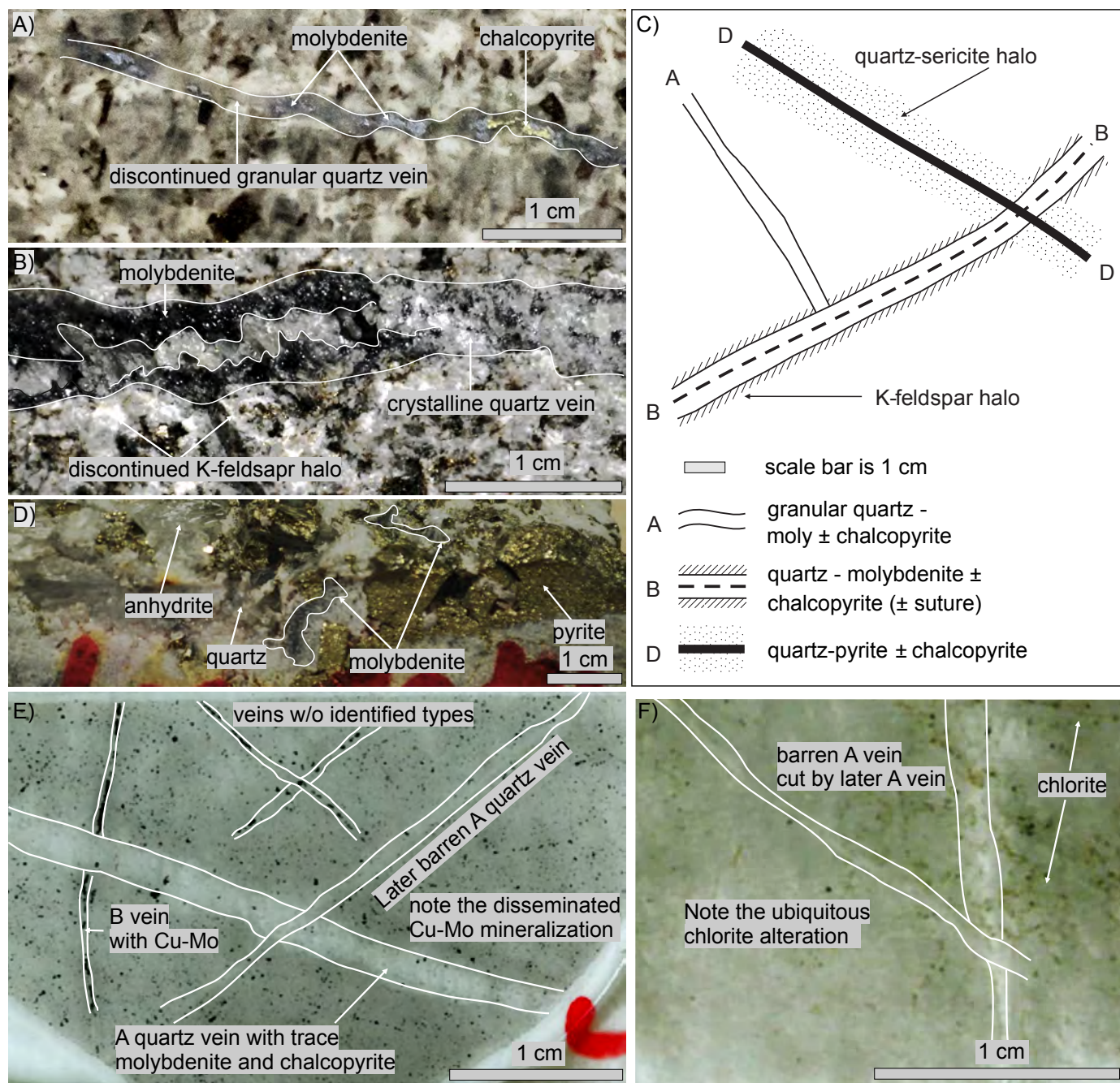


Fig. 5

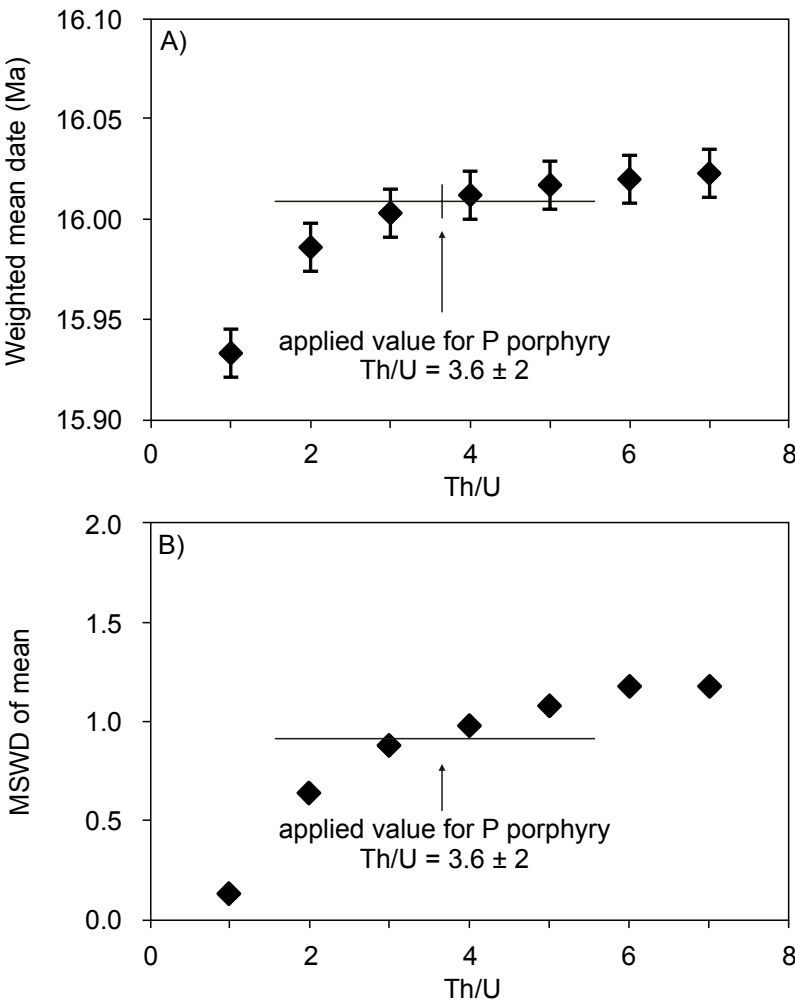


Fig. 6

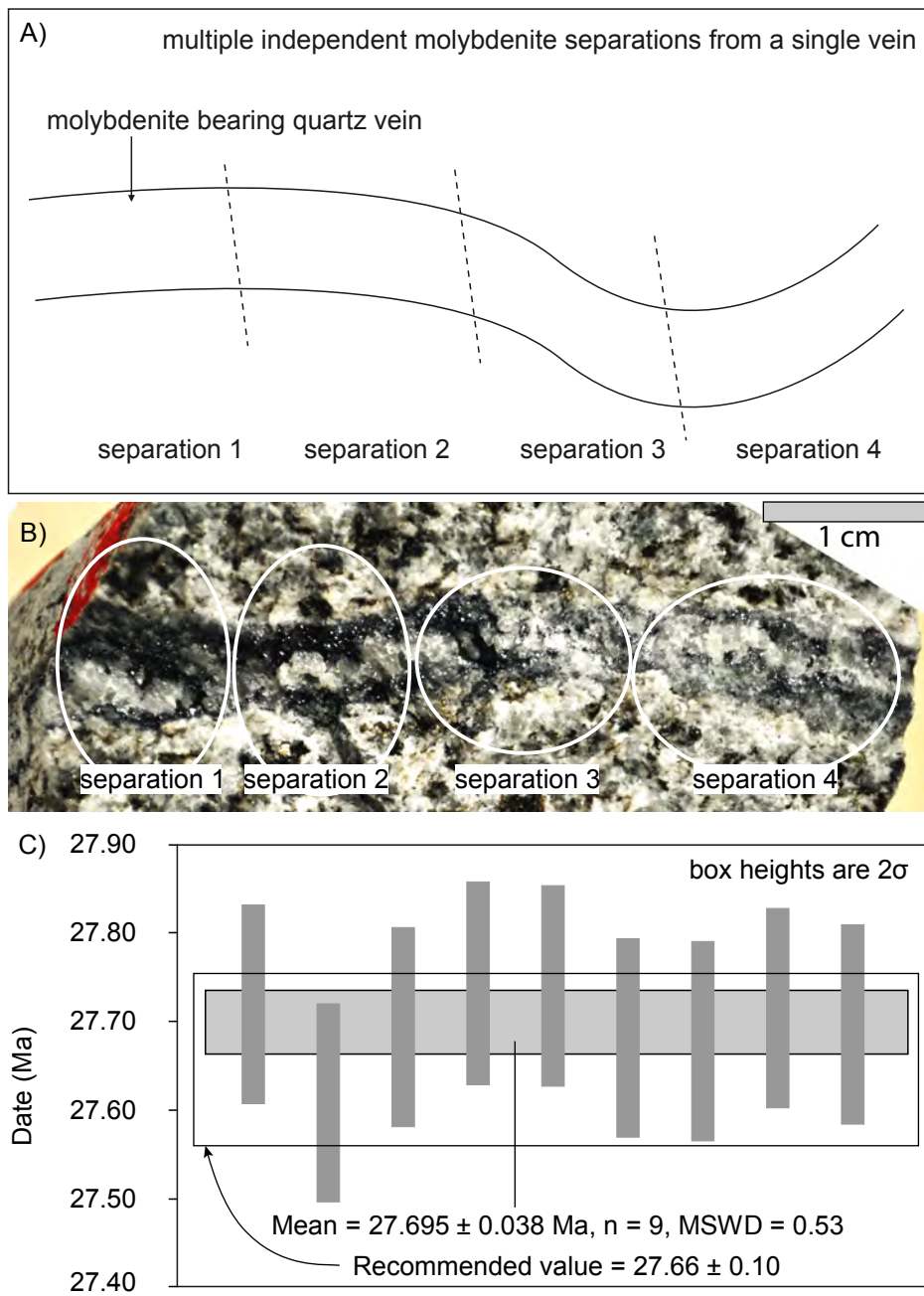


Fig. 7

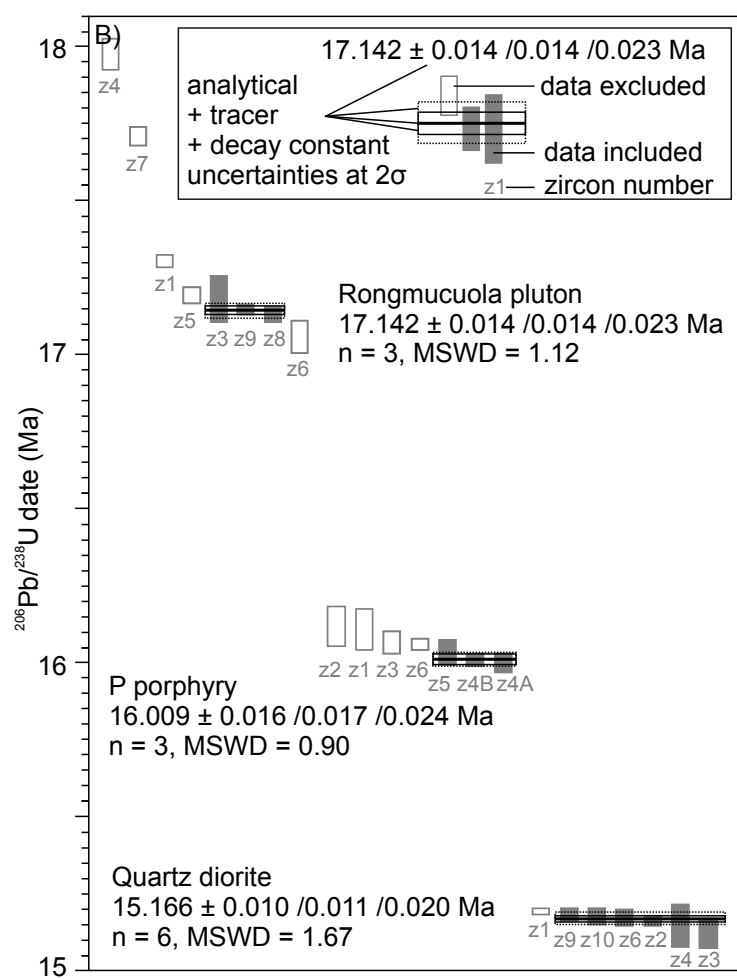
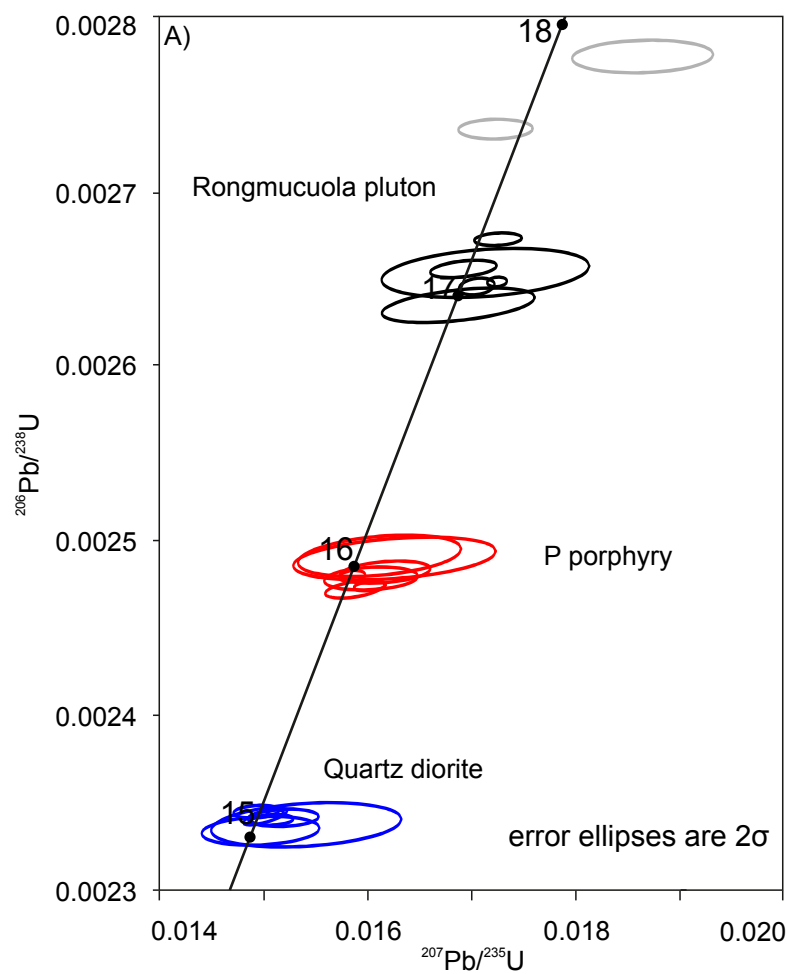


Fig. 8

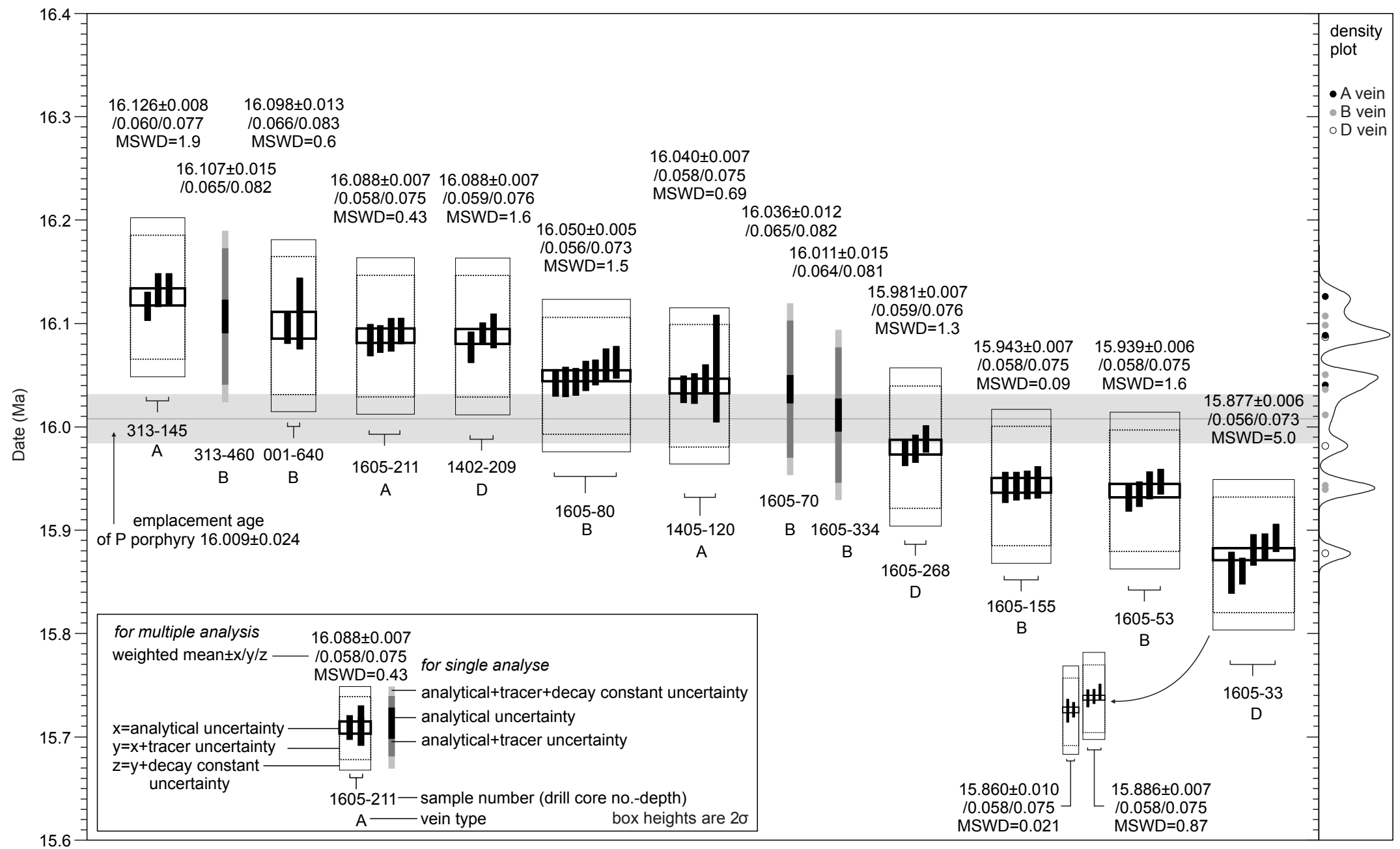


Fig. 9

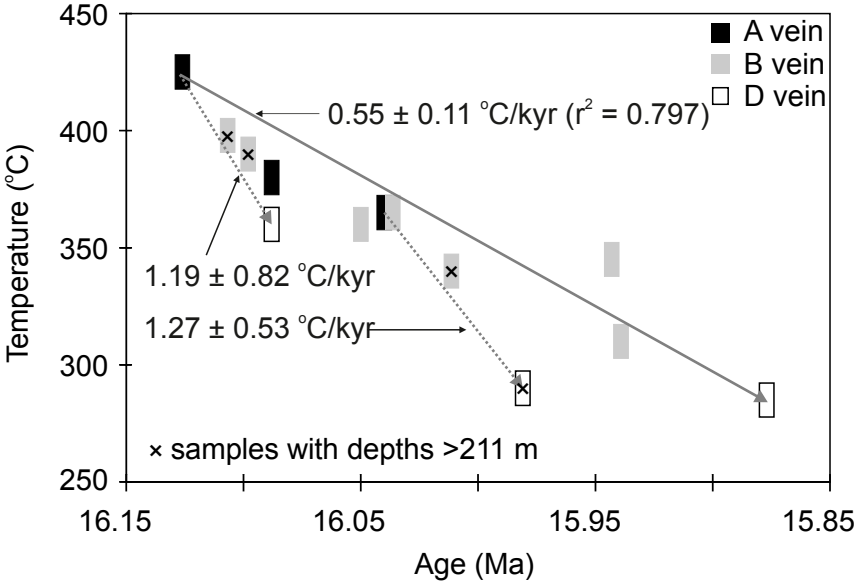


Fig. 10

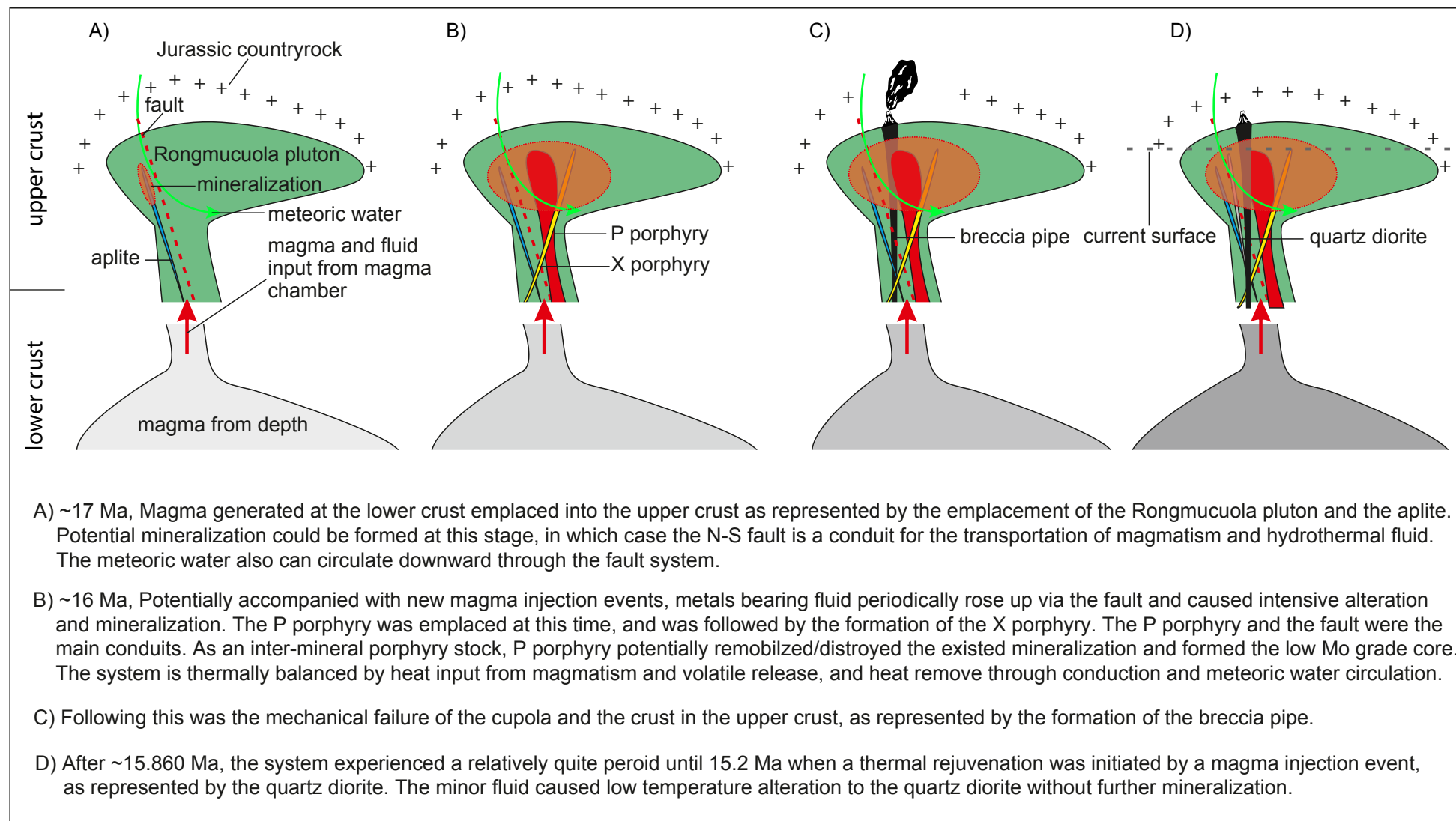


Fig. 11

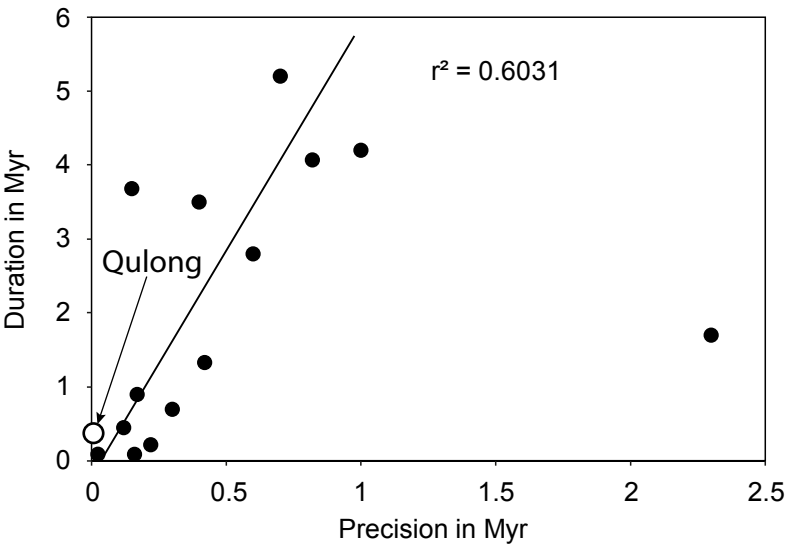




Table 1 CA-ID-TIMS U-Pb data of Miocene intrusive rocks at Qulong

		Composition					Isotopic Ratios										Dates (Ma)									
sample	Fraction	Th/ U ^d	Pb* (pg) ^e	Pbc (pg) ^f	Pb*/ Pbc ^g	Th/U[magma]	±2σ abs	²⁰⁶ Pb/ ²⁰⁴ Pb ^h	²⁰⁷ Pb/ ²³⁵ U ⁱ	±2σ %	²⁰⁶ Pb/ ²³⁸ U ⁱ	±2σ %	²⁰⁷ Pb/ ²⁰⁶ Pb ⁱ	±2σ %	²⁰⁶ Pb/ ²³⁸ U ^a	±2σ abs	²⁰⁶ Pb/ ²³⁸ U ^b	±2σ abs	²⁰⁷ Pb/ ²³⁵ U ^b	±2σ abs	²⁰⁷ Pb/ ²⁰⁶ Pb ^b	±2σ abs	discordance % ^c	Corr. coef.		
1605-296	z4	0.59	1.95	0.56	3.47	4.00	2.00	222	0.01866	3.0	0.00278	0.28	0.04873	2.9	17.975	0.050	17.882	0.049	18.768	0.552	134	69	4.2	0.122		
	z7	0.55	3.38	0.27	12.63	4.00	2.00	769	0.01724	1.7	0.00274	0.17	0.04573	1.7	17.708	0.031	17.614	0.030	17.359	0.292	-18	41	-2.0	0.065		
	z1	0.57	4.82	0.50	9.66	4.00	2.00	590	0.01727	1.1	0.00267	0.11	0.04687	1.1	17.302	0.020	17.208	0.019	17.382	0.187	41	26	0.5	0.195		
	z5	0.52	2.71	0.31	8.88	4.00	2.00	552	0.01693	1.5	0.00266	0.15	0.04626	1.5	17.193	0.027	17.098	0.026	17.050	0.261	10	36	-0.8	0.391		
	z3	0.47	0.59	0.26	2.26	4.00	2.00	156	0.01715	4.8	0.00265	0.43	0.04688	4.7	17.180	0.074	17.084	0.074	17.262	0.815	42	111	0.5	0.284		
	z9	0.52	9.02	0.35	25.94	4.00	2.00	1573	0.01726	0.5	0.00265	0.09	0.04728	0.4	17.145	0.016	17.051	0.015	17.372	0.078	62	11	1.3	0.168		
	z8	0.51	9.31	0.62	15.02	4.00	2.00	921	0.01706	0.8	0.00265	0.15	0.04679	0.8	17.129	0.026	17.034	0.025	17.177	0.140	37	19	0.3	0.245		
	z6	0.59	1.59	0.36	4.40	4.00	2.00	277	0.01688	3.6	0.00264	0.31	0.04649	3.4	17.057	0.053	16.964	0.052	17.001	0.600	22	82	-0.3	0.458		
001-550	z2	1.11	4.58	1.42	3.22	3.60	2.00	185	0.01613	4.0	0.00249	0.39	0.04697	3.9	16.115	0.065	16.040	0.062	16.245	0.640	47	92	0.8	0.335		
	z1	1.05	2.41	0.81	2.99	3.60	2.00	175	0.01627	4.9	0.00249	0.40	0.04742	4.8	16.107	0.067	16.030	0.064	16.389	0.795	69	113	1.7	0.342		
	z3	0.84	5.10	0.72	7.12	3.60	2.00	411	0.01618	2.2	0.00248	0.21	0.04730	2.1	16.063	0.036	15.979	0.033	16.297	0.356	63	51	1.4	0.306		
	z6	0.55	25.24	1.48	17.10	3.60	2.00	1036	0.01587	0.6	0.00248	0.11	0.04643	0.6	16.057	0.019	15.965	0.017	15.983	0.102	19	15	-0.5	0.204		
	z5	1.11	4.78	0.92	5.19	3.60	2.00	287	0.01605	2.3	0.00248	0.22	0.04698	2.3	16.031	0.039	15.956	0.035	16.163	0.368	47	54	0.8	0.208		
	z4B	0.94	6.07	0.30	20.33	3.60	2.00	1113	0.01603	0.8	0.00247	0.09	0.04703	0.8	16.008	0.021	15.928	0.014	16.152	0.126	50	18	0.9	0.294		
	z4A	0.92	3.40	0.33	10.20	3.60	2.00	571	0.01589	1.5	0.00247	0.17	0.04664	1.4	15.998	0.031	15.917	0.027	16.008	0.233	30	33	0.1	0.494		
1605-81	z8	1.13	1.25	1.03	1.21	4.97	2.00	80	0.03674	18.0	0.00563	1.46	0.04737	17.0	36.267	0.528	36.183	0.528	36.641	6.475	67	406	1.0	0.668		
	z1	0.50	7.23	0.30	23.78	4.97	2.00	1452	0.01513	0.4	0.00234	0.06	0.04683	0.4	15.189	0.009	15.091	0.009	15.243	0.067	39	10	0.4	0.222		
	z9	1.14	2.97	0.26	11.38	4.97	2.00	604	0.01494	1.2	0.00234	0.13	0.04625	1.2	15.179	0.019	15.095	0.019	15.061	0.179	10	28	-0.8	0.226		
	z10	0.60	3.35	0.28	11.82	4.97	2.00	713	0.01503	1.1	0.00234	0.16	0.04657	1.0	15.173	0.025	15.077	0.025	15.147	0.171	26	25	-0.2	0.717		
	z6	0.48	3.95	0.73	5.42	4.97	2.00	347	0.01520	1.8	0.00234	0.17	0.04712	1.8	15.171	0.026	15.073	0.026	15.321	0.278	54	43	1.0	0.138		
	z2	0.72	8.33	0.83	9.99	4.97	2.00	587	0.01510	1.1	0.00234	0.11	0.04682	1.1	15.158	0.016	15.065	0.016	15.215	0.165	39	26	0.4	0.166		
	z4	0.57	2.39	1.03	2.33	4.97	2.00	156	0.01542	4.8	0.00234	0.44	0.04789	4.8	15.143	0.067	15.047	0.067	15.541	0.747	93	113	2.6	0.253		
	z3	0.81	4.47	1.27	3.52	4.97	2.00	214	0.01498	3.1	0.00233	0.29	0.04660	3.0	15.116	0.044	15.025	0.044	15.102	0.462	27	73	-0.1	0.185		

^a Corrected for initial Th/U disequilibrium using radiogenic ²⁰⁸Pb and Th/U[magma]

^b Isotopic dates calculated using the decay constants λ₂₃₈ = 1.55125E-10 and λ₂₃₅ = 9.8485E-10 (Jaffey et al. 1971).

^c % discordance = 100 - (100 * (²⁰⁶Pb/²³⁸U date) / (²⁰⁷Pb/²³⁵Pb date))

^d Th contents calculated from radiogenic ²⁰⁸Pb and the ²³⁰Th-corrected ²⁰⁶Pb/²³⁸U date of the sample, assuming concordance between the U-Pb and Th-Pb systems.

^e Total mass of radiogenic Pb.

^f Total mass of common Pb.

^g Ratio of radiogenic Pb (including 208Pb) to common Pb.

^h Measured ratio corrected for fractionation and spike contribution only.

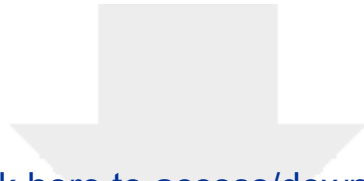
ⁱ Measured ratios corrected for fractionation, tracer and blank.

Table 2 Re-Os data of molybdenite samples from Qulong

Sample	wt (g)	Re (ppm)	2 sigma (abs)	¹⁸⁷ Re (ppm)	2 sigma abs	¹⁸⁷ Os (ppb)	2 sigma abs	Date (Ma)	2 sigma abs	average (Ma)	2 sigma abs uncertainties			vein type	depth (meter)	Temperature (°C) ^d
313-145_3-3*	0.021	64.4	0.2	40.4	0.2	10.9	0.0	16.117	0.006							
313-145_2-3	0.011	59.6	0.3	37.4	0.2	10.1	0.0	16.132	0.008	16.126	0.008	0.060	0.077	A	145	425
313-145_1-3	0.042	66.0	0.2	41.5	0.1	11.1	0.0	16.133	0.007							
313-460*	0.014	143.3	0.6	90.1	0.4	24.2	0.1	16.107	0.008	16.107	0.015	0.065	0.082	B	460	398
001-640*	0.010	104.2	0.5	65.5	0.3	17.6	0.1	16.096	0.007							
001-640_2-2	0.021	99.7	0.4	62.7	0.2	16.8	0.1	16.110	0.017	16.098	0.013	0.066	0.083	B	640	390
1605-211_3-4	0.042	210.2	0.7	132.1	0.4	35.4	0.1	16.084	0.007							
1605-211_1-4	0.032	226.8	0.8	142.6	0.5	38.2	0.1	16.085	0.006	16.088	0.007	0.058	0.075	A	211	360
1605-211_2-4	0.030	239.3	0.8	150.4	0.5	40.3	0.1	16.089	0.008							
1605-211_4-4	0.040	247.9	0.8	155.8	0.5	41.8	0.1	16.093	0.006							
1402-209_1-3	0.022	274.5	1.0	172.5	0.6	46.2	0.1	16.077	0.007							
1402-209_3-3	0.020	454.3	1.7	285.5	1.1	76.6	0.2	16.091	0.005	16.088	0.007	0.059	0.076	D	209	380
1402-209_2-3	0.044	257.4	0.8	161.8	0.5	43.4	0.1	16.093	0.008							
1605-80_1-7	0.038	421.3	1.4	264.8	0.9	70.8	0.2	16.042	0.006							
1605-80_3-7	0.051	434.0	1.4	272.8	0.9	72.9	0.2	16.043	0.007							
1605-80_2-7	0.053	437.2	1.4	274.8	0.9	73.5	0.2	16.043	0.006							
1605-80_5-7	0.048	435.0	1.4	273.4	0.9	73.1	0.2	16.049	0.007	16.050	0.005	0.056	0.073	B	80	360
1605-80_4-7	0.071	466.4	1.5	293.1	0.9	78.4	0.2	16.053	0.006							
1605-80_7-7	0.050	435.3	1.4	273.6	0.9	73.2	0.2	16.060	0.007							
1605-80_6-7	0.050	411.1	1.3	258.4	0.8	69.2	0.2	16.062	0.007							
1405-120_2-4	0.020	250.6	0.9	157.5	0.6	42.1	0.1	16.036	0.006							
1405-120_4-4	0.013	259.7	1.2	163.3	0.7	43.6	0.2	16.037	0.007	16.040	0.007	0.058	0.075	A	120	365
1405-120_1-4	0.021	250.2	0.9	157.3	0.6	42.1	0.1	16.047	0.006							
1405-120_3-4	0.012	261.8	1.3	164.5	0.8	44.0	0.2	16.056	0.025							
1605-70	0.013	125.2	0.5	78.7	0.3	21.0	0.1	16.036	0.006	16.036	0.012	0.065	0.082	B	70	365
1605-334*	0.039	224.5	0.7	141.1	0.5	37.6	0.1	16.011	0.007	16.011	0.015	0.064	0.081	B	334	340
1605-268_2-3	0.013	492.7	2.2	309.7	1.4	82.4	0.3	15.975	0.006							
1605-268_3-3	0.022	504.0	1.8	316.8	1.2	84.3	0.3	15.979	0.006	15.981	0.007	0.059	0.076	D	268	290
1605-268_1-3	0.024	504.0	1.8	316.7	1.1	84.4	0.3	15.988	0.006							
1605-155_3-4	0.023	172.0	0.6	108.1	0.4	28.7	0.1	15.941	0.007							
1605-155_2-4	0.031	137.2	0.5	86.2	0.3	22.9	0.1	15.943	0.006	15.943	0.007	0.058	0.075	B	155	345
1605-155_1-4*	0.020	232.9	0.9	146.4	0.5	38.9	0.1	15.944	0.006							
1605-155_4-4	0.019	210.9	0.8	132.6	0.5	35.2	0.1	15.946	0.007							
1605-53_4-4	0.011	372.9	1.8	234.3	1.1	62.2	0.3	15.931	0.006							
1605-53_1-4	0.030	401.5	1.4	252.4	0.9	67.0	0.2	15.935	0.005	15.939	0.006	0.058	0.075	B	53	310
1605-53_2-4	0.017	348.0	1.4	218.7	0.9	58.1	0.2	15.943	0.006							
1605-53_3-4	0.012	395.3	1.8	248.5	1.1	66.0	0.3	15.947	0.006							
1605-33_3-5	0.013	310.7	1.4	195.3	0.9	51.6	0.2	15.859	0.010							
1605-33_1-5	0.045	311.9	1.0	196.1	0.6	51.8	0.1	15.860	0.006							
1605-33*	0.012	323.6	1.5	203.4	0.9	53.8	0.2	15.881	0.007	15.860	0.010	0.058	0.075	D	33	285
1605-33_2-5	0.024	298.7	1.1	187.7	0.7	49.7	0.1	15.884	0.006							
1605-33_4-5	0.020	284.1	1.1	178.6	0.7	47.3	0.1	15.892	0.006							

^aanalytical uncertainty^banalytical and tracer uncertainty^canalytical, tracer and decay constant uncertainty of Smoliar et al., 1996^dvein formation temperatures constrained by fluid inclusion study from Li et al., 2017

*data reprocessed (re-run the Re separations or digest a new aliquot of the same mineral separations) after LI et al 2017, Mineralium Deposita



[Click here to access/download](#)

Electronic Appendix (Excel etc.)
4_appendix.pdf

